

1 **Characterization of Ozone Profiles Derived from Aura TES**
2 **and OMI Radiances**

3

4 **Dejian Fu¹, John R. Worden¹, Xiong Liu², Susan S. Kulawik¹, Kevin W.**
5 **Bowman¹, Vijay Natraj¹**

6

7 [1]{Earth and Space Sciences Division, Jet Propulsion Laboratory, California Institute of
8 Technology, Pasadena, California, 91109, USA}

9 [2]{Harvard-Smithsonian Center for Astrophysics, Cambridge, Massachusetts, 02138, USA}

10 Correspondence to: D. Fu (dejian.fu@jpl.nasa.gov)

11

12 **Abstract**

13 We present satellite based ozone profile estimates derived by combining radiances measured
14 at thermal infrared (TIR) wavelengths from the Aura Tropospheric Emission Spectrometer
15 (TES) and ultraviolet (UV) wavelengths measured by the Aura Ozone Monitoring Instrument
16 (OMI). The advantage of using these combined wavelengths and instruments for sounding
17 ozone over either instrument alone is improved sensitivity near the surface as well as the
18 capability to consistently resolve the lower troposphere, upper troposphere, and lower
19 stratosphere for scenes with varying geophysical states. For example, the vertical resolution
20 of ozone estimates from either TES or OMI varies strongly by surface albedo and
21 temperature. Typically TES provides 1.6 degrees-of-freedom for signal (DOFS) and OMI
22 provides less than 1 DOFS for OMI in the troposphere. The combination provides 2 DOFS in
23 the troposphere with approximately 0.4 DOFS for near surface ozone (surface to 700 hPa).
24 We evaluated these new ozone profile estimates with ozonesonde measurements and found
25 that calculated errors for the joint TES and OMI ozone profile estimates are in reasonable
26 agreement with actual errors as derived by the root-mean-square (RMS) difference between

1 the ozonesondes and the joint TES/OMI ozone estimates. We also used a common a priori
2 profile in the retrievals in order to evaluate the capability of different retrieval approaches on
3 capturing near-surface ozone variability. We found that the vertical resolution of the joint
4 TES/OMI ozone profile estimates show significant improvements on quantifying variations in
5 near-surface ozone with RMS differences of 49.9% and correlation coefficient of $R = 0.58$ for
6 the TES/OMI near-surface estimates as compared to 73.6% RMS difference and $R = 0.33$ for
7 TES and 115.8% RMS difference and $R = 0.09$ for OMI. This comparison removes the
8 impacts of the climatological a priori on the comparison and results in artificially large
9 sonde/retrieval differences. The TES/OMI ozone profiles from the production code of joint
10 retrievals will use climatological priors and therefore will have more realistic ozone estimates.

11

12 **1 Introduction**

13 The vertical distribution of ozone plays important roles in the Earth's atmosphere since ozone
14 filters out bio-damaging ultraviolet (UV) light (wavelength < 280 nm) in the stratosphere, acts
15 as a greenhouse gas in the upper troposphere, regulates the oxidation capacity of the lower
16 atmosphere, and affects the air quality for humans and vegetation near the Earth's surface.
17 About 90% of the total atmospheric ozone is in the stratosphere with the remaining 10% in
18 the troposphere where it acts as a greenhouse gas in the upper troposphere and as a pollutant
19 near the surface. For example, exposure to ozone gas can harm lung function, irritate the
20 respiratory system (WHO 2003; Bell et al., 2006) and increase the risk of death from
21 respiratory causes (Jerrett et al., 2009; Weinhold, 2008). Ozone and pollution at ground level
22 interfere with photosynthesis and stunt overall growth of plants and consequently can reduce
23 agricultural yields (Hatfield et al., 2008).

24 Quantifying the vertical distribution of ozone is needed to investigate the mechanisms that
25 control ozone concentration. *In situ* and remote sensing techniques have been used in the
26 measurements of ozone vertical distributions. The ozonesonde (Komhyr et al., 1995) is a
27 lightweight (~ 700 g), compact ($19.1 \times 19.1 \times 25.4$ cm), balloon-borne, *in situ* instrument that
28 provides measurements with a high vertical resolution (~ 150 m) and accuracy (~ 5 -10%) over
29 regional scales. Remote sensing of ozone concentration using spectroscopic techniques has
30 been performed using both UV and TIR measurements. The UV measurements were carried
31 out from ground (Götz et al., 1934; McDermid et al., 2002; Petropavlovskikh et al., 2005;

1 Tzortziou et al., 2008), aircraft (Browell et al., 1983), balloon (Weidner et al., 2005), and
2 spaceborne platforms (nadir-viewing measurements by SBUV (Bhartia et al., 1996), GOME
3 (Munro et al., 1998; Hoogen et al., 1999; Liu et al., 2005, 2006), GOME-2 (van Peet et al.,
4 2009; Cai et al., 2012), OMI (Liu et al., 2010a; Kroon et al., 2011) and limb-scattering
5 measurements by SOLSE (McPeters et al., 2000), OSIRIS (von Savigny et al., 2003),
6 SCIAMACHY (Eichman et al., 2004; Sellitto et al., 2012a,b)). The TIR measurements were
7 performed from ground (Hamdouni et al., 1997; Pougatchev et al., 1995), aircraft (Toon et al.,
8 1989; Blom et al., 1995), balloon (Clarmann et al., 1993; Toon et al. 2002), and spaceborne
9 platforms (CRISTA (Riese et al., 1999), ATMOS (Gunson et al., 1990), CLAES (Bailey et
10 al., 1996), HALOE (Brühl et al., 1996), ACE-FTS (Bernath et al., 2005; Boone et al., 2005),
11 and TES (Beer et al., 2001, Beer 2006; Bowman et al., 2006), IASI (Clerbaux et al., 2010)).

12 In the UV, the backscattered radiance spectra measured from space contain information on
13 the vertical distribution of ozone because of the dependency of ozone absorption on
14 wavelength and attenuation of UV through Rayleigh scattering (Chance et al., 1997). The
15 ozone ν_3 band around 9.6 μm is useful for profiling atmospheric ozone distributions because
16 the rotation-vibration resolved spectral lines of the ν_3 band depend on pressure and
17 temperature. Both TIR and UV sounders are able to provide information on tropospheric
18 ozone concentration, although UV sounders show less vertical information in the troposphere
19 and more vertical information in the stratosphere compared to IR sounders because the UV
20 lines are less sensitive to temperature and pressure.

21 Recent studies point towards the potential of combining radiances measured in multiple
22 spectral regions for increasing the vertical resolution of tropospheric trace gases. Worden et
23 al. (2007b) performed synthetic retrievals for three instruments whose characterizations are
24 similar to TES, OMI, and the combination of TES and OMI. The study demonstrated that
25 estimating ozone profiles by combining UV (270–340 nm) and TIR (ozone band near 9.6 μm)
26 radiances yields a factor of two or more improvement in the ability to resolve boundary layer
27 ozone, compared with either instrument alone. In addition, there is a substantial improvement
28 in the vertical resolution of ozone in the free troposphere (between 20% and 60%) as
29 compared to the TES vertical resolution. Landgraf and Hasekamp (2007) investigated the
30 synergistic use of TIR (ozone band near 9.6 μm) and UV spectral region (290–320 nm) for
31 the retrieval of vertical distribution of tropospheric ozone from satellite observations. The
32 study also led to the conclusion that combining TIR and UV spectral ranges can improve

1 significantly the retrieved ozone in the lowest 5 km of the troposphere. Using simulated
2 measurements for 16 cloud and aerosol free atmospheric profiles spanning a range of ozone
3 mixing ratios, Natraj et al. (2011) explored the feasibility of using multi-spectral intensity
4 measurements in the UV, visible (VIS), mid-infrared (MIR) and TIR, also utilizing
5 polarization measurements in the UV/VIS to improve tropospheric and lowermost
6 tropospheric ozone measurements (surface to 2 km above surface). The analysis suggested
7 that UV + VIS, UV + TIR and UV + VIS + TIR combinations have the potential to satisfy the
8 measurement requirements (two degrees of freedom in the troposphere, and sensitivity from
9 surface to 2 km) of the Geostationary Coastal and Air Pollution Events (GEO-CAPE)
10 mission, a National Research Council recommended mission identified in "Earth Science and
11 Applications from Space: National Imperatives for the Next Decade and Beyond" (National
12 Research Council 2007; Fishman et al., 2012). In addition to the NASA GEO-CAPE mission,
13 Korea GEMS (Geostationary Environment Monitoring Spectrometer [Lee et al., 2010])
14 mission, Japanese GMAP-Asia (Geostationary Meteorology and Air Pollution-Asia [Akimoto
15 et al. 2008]) mission, European GMES (Global Monitoring for Environment and Security)
16 sentinels-4 and -5 missions (Lahoz *et al.*, 2012; Ingmann *et al.*, 2012; ESA, 2007) have been
17 proposed for the air quality application. The Canadian PCW/PHEMOS-WCA (Polar
18 communication and Weather/Polar Highly Elliptical Molniya Orbital Science - Weather,
19 Climate and Air quality [McConnell et al., 2011]) mission proposed to use UV-VIS-TIR
20 spectrometers onboard two satellites each in a highly eccentric orbit (apogee: ~42,000 km;
21 period: 12-24 hour) to provide air quality measurements over polar regions where GEO
22 missions have poor coverage. The constellation of European, United States, Asian GEO
23 missions and the Canadian PCW/PHEMOS-WCA mission, provide global monitoring of air
24 quality with proposed launch dates between 2017 to 2020. These proposed GEO missions
25 likely will use a multispectral approach such as the use of TIR with other spectral regions
26 (such as UV, VIS, NIR) to obtain near-surface estimates of CO and ozone. [In this paper, we](#)
27 [explore the feasibility of estimating ozone using multiple spectral bands by using the](#)
28 [measurements from the EOS-Aura mission. In addition to our work, Cuesta et al. \(2013\)](#)
29 [developed a multiple spectral retrieval algorithm on tropospheric ozone soundings using IASI](#)
30 [and GOME-2 simultaneously measured radiances from the MetOp satellite in the sun-](#)
31 [synchronous orbit \(local time of ascending node: 9:31 am\). Both this work and Cuesta et al.](#)
32 [\(2013\) used identical spectral regions of the \$\nu_3\$ band in TIR and the Hartley and Huggins](#)
33 [bands in the UV and showed similar vertical sensitivities and measurement uncertainties of](#)

1 ozone profile estimates.

2 The intuitive explanation of why multispectral satellite retrievals enhance near-surface
3 sensitivity to trace gas concentrations is that the reflected UV sunlight radiances are sensitive
4 to the tropospheric column whereas the TIR sounders are primarily sensitive to the free-
5 troposphere. The “subtraction” of the free tropospheric estimates from the total column
6 estimates results in an estimate of near-surface concentrations. This “subtraction” must be
7 performed using a non-linear retrieval for strongly varying trace gasses such as ozone as
8 discussed here and in Worden *et al.* (2007) or CO (Worden *et al.*, 2010) but can be performed
9 linearly for weakly varying trace gasses such as CO₂ (Kuai *et al.*, 2012).

10 In this paper, we show ozone profile results using radiance measurements from both the TES
11 and OMI instruments. The paper is organized as follows: Section 2 describes the TES, OMI
12 and ozonesonde measurements used in this work; Section 3 provides details of the retrieval
13 algorithm; Section 4 discusses the retrieval characterization of these multispectral retrievals,
14 and shows examples of retrievals with a focus on tropospheric ozone and compares joint TES
15 and OMI retrieval characteristics with those of using either instrument alone. Section 5
16 provides conclusions.

17

18 **2 TES, OMI, and Ozonesonde Measurements**

19 Both TES and OMI instruments are on the NASA Aura platform launched in 2004 in a near-
20 polar, sun-synchronous, 705 km altitude orbit whose ascending node has a 1:38 pm equator
21 crossing time.

22 **2.1 TES Measurements**

23 TES is a Fourier transform spectrometer that measures radiances in the TIR (650–3050 cm⁻¹)
24 at a spectral resolution of 0.1 cm⁻¹ for nadir viewing. A single TES nadir measurement takes 4
25 seconds and has a footprint size of 5.3 km (across track) × 8.5 km (along the spacecraft
26 ground track). During each measurement, TES “stares” at the observation location
27 compensating for spacecraft motion. The TES instrument observes the Earths’ TIR radiance
28 in four spectral ranges using a separate array of detectors identified as 1A, 1B, 2A, and 2B.
29 TES atmospheric measurements of 1B2 (950–1150 cm⁻¹) subregions have high-density

1 absorption features of the ozone ν_3 band (the strongest fundamental band) and minor
2 absorption from interfering species, providing sensitivity for estimating atmospheric ozone
3 volume mixing ratio (VMR). H₂O absorption features spread across the TIR spectra and need
4 to be taken into account when estimating ozone VMR. Therefore, TES 2A1 (1100–1325 cm⁻¹)
5 measurements were used to estimate H₂O VMR. Table 1 lists the spectral windows that were
6 used in our retrievals. TIR radiances in units of watts per square centimeter per steradian per
7 inverse centimeter (W/cm²/sr/cm⁻¹), with associated estimates of random error named noise
8 equivalent spectral radiance (NESR), were used in the retrievals. Both radiances and NESR
9 were obtained from the processes of phase correction and radiometric calibration using TES
10 level 1 algorithms (Worden et al., 2006). TES has two science-operating modes: Global
11 Surveys (GS) and Special Observations (SO). GS are the observations that TES conducts
12 approximately every two days and provides global measurements of atmospheric
13 composition. The SO mode includes targeted measurements used for validation activities or to
14 examine regional processes and emissions. Beer et al. [2001] and Beer [2006] described the
15 TES instrument and data acquisition modes in detail. To obtain radiances that were taken co-
16 located to OMI measurements, we used TES nadir measurements in either GS or SO mode
17 over sonde sites.

18 2.2 OMI Measurements

19 OMI is a nadir-viewing push broom ultraviolet-visible (UV-VIS) imaging spectrograph that
20 measures backscattered radiances covering the 270–500 nm wavelength range. The spectral
21 range is divided into three subregions identified as UV-1 (270–310 nm), UV-2 (310–365 nm)
22 and VIS (365–500 nm). Retrievals presented in this paper used portions of the UV-1 (270–
23 308 nm) and UV-2 (312–330 nm) spectral ranges, where the absorption features of the ozone
24 Hartley and Huggins bands are clearly present in the spectra recorded by OMI. OMI has
25 global measurement, spectral and spatial zoom-in modes. The ground pixel size at nadir
26 position in the global mode (swath width about 2600 km) is 13 km (along the ground track of
27 spacecraft) × 24 km (across track) for the UV-2 and VIS channels, and 13 km (along the
28 ground track of spacecraft) × 48 km (across track) for the UV-1 channel. Two UV-2 spectra
29 are co-added to match the UV-1 spatial resolution. OMI zoom-in mode measurements are not
30 included in this work due to lack of coincident TES and ozonesonde measurements. Row
31 anomaly and stray light issues affect the quality of OMI measured radiance data. Since 2009,
32 these instrument issues severely affected OMI measurements, which were collated to TES

1 measurements. For this reason, the TES and OMI joint retrievals shown in our study are for
2 measurements from 2005 to 2008.

3 **2.3 Ozonesonde Measurements**

4 Ozonesonde measurements that provide in situ data from the surface to the stratosphere
5 (about 35 km) with vertical resolution of ~150 m and accuracy of $\pm 5\%$ fill a critical need for
6 the validation of ozone profiles measured by TES and OMI instruments. The ozonesonde
7 sensor has a dilute solution of potassium iodide to produce a weak electrical current
8 proportional to the ozone concentration of the sampled air (Komhyr et al., 1995). To examine
9 the performances of TES, OMI and sonde in capturing the variations of surface ozone
10 concentration, we applied the following coincidence criteria to select sonde-TES-OMI pairs:
11 mean cloud optical depth < 0.1 , distance among TES, OMI and sonde < 50 km, and time
12 difference < 1 hour. Using these criteria for the September 2004 to December 2008
13 timeframe, we obtained 22 sonde-TES-OMI measurement triads (Table 2).

14

15 **3 Joint TES and OMI O₃ retrievals**

16 **3.1 Radiative Transfer Calculation**

17 The retrieval strategy utilizes a non-linear least squares method to minimize the difference
18 between observed and calculated spectral radiances subject to second-order statistical
19 constraints on the variability of the atmospheric state (Bowman et al, 2002, Kulawik et al.
20 2006a). A critical requirement for a forward model is that it be as accurate as possible and be
21 capable of performing the calculations with acceptable computational cost (Clough et al.,
22 2006). The OMI ozone vertical profiles have been retrieved/validated by Liu et al. (2010a,b).
23 To reduce the amount of effort to program and validate a new model for the TIR spectral
24 region, the joint TES and OMI forward model uses the forward model component of the Earth
25 Limb and Nadir Operational Retrieval prototype (IDL-ELANOR) to simulate spectral
26 radiances and Jacobians (sensitivity of spectral radiance measured by the instrument to
27 perturbations in retrieved parameters). In the UV spectral region, we use the Vector
28 Linearized Discrete Ordinate Radiative Transfer (VLIDORT) model (Spurr 2006, 2008), with

1 configurations similar to those in Liu et al. (2010a), to compute the spectral radiances and
2 Jacobians.

3 **3.1.1 Radiative Transfer Calculation for the TIR**

4 The TES operational retrieval algorithm simulates TIR spectral radiances using its forward
5 model component and adjusts the state vector being estimated to minimize the differences
6 between the measured spectral radiances and those obtained from the forward model subject
7 to a priori constraints on the mean and covariance of the atmospheric state. The forward
8 model component does line-by-line radiative transfer modeling, which includes upwelling
9 atmospheric emission, downwelling and back-reflected atmospheric emission, and surface
10 emission (Clough et al., 2006), and cloud properties (Kulawik et al., 2007; Eldering et al.,
11 2008). It also simulates the [characteristics](#) of the TES instrument. It provides simulated
12 radiances and Jacobians of the spectral radiances with respect to specified parameters.

13 The radiative transfer calculation in the forward model uses a 66-layer pressure grid at fixed
14 pressure levels. The pressure at the Earth's surface provides the lower boundary for the
15 forward model and is defined for every TES observation. The sea surface pressure is obtained
16 from the Global Modeling and Assimilation Office (GMAO) GEOS-5 (Goddard Earth
17 Observing System Model, version 5) model (Molod et al, 2012). The surface pressure is
18 calculated from the sea surface pressure using the hydrostatic equation at the surface geodetic
19 elevation. The top pressure boundary for the surface layer is a TES fixed pressure level.

20 For the simulation of ozone spectral radiances and weighting functions in the [TIR](#) spectral
21 region (Table 1), we used the line positions, intensities and broadening parameters from
22 Wagner et al. (2002). Those spectroscopic parameters have been used by the MIPAS mission
23 (Flaud et al., 2003) and been included in the [HITRAN 2004 database \(High-resolution](#)
24 [TRANsmission molecular absorption database\)](#) (Rothman et al., 2005, 2009). The accuracy of
25 the line intensities is about 3%.

26 For the TIR spectral region, the contribution of clouds in the radiative transfer modeling is
27 parameterized in terms of a set of frequency-dependent nonscattering optical depths and a
28 cloud top pressure (Clough et al., 2006; Kulawik et al., 2006b; Eldering et al., 2008). The
29 model assumes clouds that are distributed about a single pressure level, which is denoted by
30 the cloud top pressure. These cloud parameters are retrieved jointly with surface temperature,

1 emissivity, atmospheric temperature, and trace gases such as ozone from TES TIR spectral
2 data.

3 **3.1.2 Radiative Transfer Calculation for the UV**

4 We [used](#) VLIDORT as the core of the forward model in the UV spectral region for the
5 numerical computation of the Stokes vector in a multiple-scattering multilayer medium. This
6 model uses the discrete ordinate method to approximate the multiple scatter integrals (Spurr
7 2006, 2008). VLIDORT accounts for sphericity in the treatments of the incoming solar beam
8 and outgoing beam attenuations. It calculates the Stokes parameters I, Q, U and V for a given
9 model atmosphere, spectroscopic parameters and viewing geometry. For the calculations
10 performed in this paper, VLIDORT was run in full-polarization mode. We expect that the
11 effect of OMI instrument polarization sensitivity on the measured radiances is negligible
12 since it utilizes a polarization scrambler to depolarize the measurement signal. The Jacobians
13 with respect to the atmospheric trace gas concentration and surface properties are computed
14 analytically by VLIDORT. Liu et al. (2010a) developed a retrieval algorithm, which uses
15 VLIDORT as the forward model, to obtain O₃ VMR profiles using OMI measurements. A
16 single scattering model (Sioris and Evans, 2000) was used to simulate the Ring effect. For
17 simulating radiances measured by OMI, we adopt [the configurations](#) that have been used in
18 Liu's retrieval algorithm, to optimize radiative transfer calculations in the UV spectral region.

19 The radiances [were](#) calculated for a Rayleigh atmosphere (no aerosols) with Lambertian
20 reflectance assumed for the surface. We [used](#) the surface reflectance climatology constructed
21 using 3 years of OMI measurements [obtained](#) between 2004 and 2007 (Kleipool et al., 2008).
22 The surface albedo in UV-2 is wavelength-dependent and is represented as first-order
23 polynomials, which represent the surface effects and partly account for the presence of
24 aerosols (similar to using climatological aerosols). Although higher-order polynomials can
25 further reduce fitting residuals, they can adversely impact retrieval accuracy due to overly
26 strong correlation with ozone. In the spectral region of interest, atmospheric SO₂ and BrO
27 absorption is typically much weaker than that of O₃. They [were](#) not modeled or retrieved. This
28 only slightly affects retrievals except for volcanic eruption conditions. Simulations and
29 retrievals of SO₂ and BrO will be added later, since there is adequate spectral information in
30 our fitting window for these trace gases. High-resolution (0.01 nm) ozone cross sections
31 (Brion et al., 1993) [were](#) used in the simulation, which [had](#) been found to significantly reduce

1 fitting residuals in the Huggins band compared to other cross sections (Liu et al., 2007). The
2 simulated high spectral resolution radiances and Jacobians **were** convolved with the OMI
3 instrument slit function, which **was** computed using the hyper-parameterization parameters
4 obtained during the on-ground calibration measurements (Dobber et al., 2006). To account for
5 the temperature dependence of ozone absorption, we **used** temperature profiles from TES
6 version 4 products.

7 Clouds **were** treated as reflecting boundaries with a Lambertian reflectance whose surface
8 albedo is 0.8. Two sets of cloud products are available from OMI measurements. One set of
9 cloud top pressure and cloud fraction **was** obtained using the O₂-O₂ absorption band near 477
10 nm (Acarreta et al., 2004) and the other set **was** retrieved using the effects of rotational
11 Raman scattering (Joiner and Vasilkov, 2006; Vasilkov et al., 2008). Having two sets of OMI
12 cloud products is to improve the temporal coverage of OMI cloud information since cloud
13 information might not be available due to the quality control of cloud retrievals. Combining
14 two sets of OMI cloud products **increases** the throughput of trace gas retrievals.

15 In the OMI-only retrievals (Liu et al., 2010a) and our work presented here, aerosols, clouds,
16 and surface pressure **were** either not accurately known or **were** not modeled in the retrievals.
17 In addition, OMI radiances need additional calibration corrections for profile retrievals. To
18 account for these effects, we **applied** radiance calibration factors to the calculated radiances
19 and fit wavelength-dependent surface albedo (i.e., zero order for UV-1, first-order
20 polynomials for UV-2) as tuning parameters. The radiance calibration factors, which **were**
21 taken from the work done by Liu et al. (2010a), **were** represented as a two-dimensional matrix
22 defined by wavelength and OMI ground pixel index (across satellite ground track direction).
23 The radiance calibration factors were derived by examining the averaged differences between
24 OMI measured radiances and simulated radiances. OMI measurements over tropics were used
25 in obtaining calibration factors since the spatiotemporal variability in ozone is smaller here
26 than in other latitude regions. The OMI radiance simulations were made using the ozone
27 profiles that were constructed as follows: zonal mean v2.2 ozone profiles (Livesey et al.,
28 2008) from the microwave limb sounder (MLS, onboard Aura satellite) for pressure < 215
29 hPa and climatological ozone profiles from McPeters et al. (2007) for pressure > 215 hPa.
30 The radiance calibration factors show significant wavelength and cross-track dependencies
31 together with discontinuities of 3–9% at 310 nm between UV-1 and UV-2.

1 There are a few differences in forward model settings between Liu et al. (2010a) and our
 2 work. VLIDORT can be run in scalar-mode only, i.e., without taking polarization into
 3 account, to reduce computation time. Liu et al. (2010a) performed scalar-only and full-
 4 polarization calculations at ~ 10 selected wavelengths to derive polarization corrections at
 5 these wavelengths, and then interpolated the polarization corrections to the entire wavelength
 6 grid of the forward model. Next, they performed scalar-only calculations for the entire
 7 wavelength grid of the forward model and applied the polarization correction factors. Liu et
 8 al. (2010a) co-added 5 and 2 adjacent spectral pixels in UV-1 and UV-2, respectively, to
 9 speed up the retrievals. Neither co-adding adjacent spectral pixels nor simulating spectral
 10 radiances in scalar mode was applied in our retrieval algorithm because the number of
 11 coincident TES and OMI measurements is similar to that of TES measurements, which is
 12 about 100 times smaller than that of OMI. Liu's OMI forward model used the daily National
 13 Center for Environmental Prediction (NCEP) reanalysis temperature profiles (Kalnay et al.,
 14 1996) with updated surface pressure derived from the topographical altitude of the OMI pixel
 15 by assuming a standard sea level pressure of 1 atm (Liu et al., 2010a). In our retrieval, we
 16 used temperature and trace gas concentration profiles from TES version 4 products for
 17 spectral simulations in both TIR and UV spectral regions.

18 **3.2 Optimal Estimation Retrievals**

19 The joint TES and OMI retrieval algorithm is based on the optimal estimation method
 20 (Bowman et al. 2002; Rodgers, 2000) that combines the a priori knowledge, which includes
 21 both a mean state and its covariance before the measurements are taken, and the information
 22 from combined TIR and UV measurements. The algorithm involves finding the best estimate
 23 state vector $\hat{\mathbf{z}}$ by minimizing the cost function shown in equation 1,

$$24 \quad \chi^2 = \|\mathbf{L}_{\text{obs}} - \mathbf{L}_{\text{sim}}(\hat{\mathbf{z}})\|_{\mathbf{S}_\epsilon}^2 + \|\mathbf{z} - \mathbf{z}_a\|_{\mathbf{S}_a}^2. \quad (1)$$

25 Equation 1 is a sum of quadratic functions representing the Euclidean distance, with the first
 26 term representing the difference between observed (\mathbf{L}_{obs}) and simulated radiance spectra
 27 ($\mathbf{L}_{\text{sim}}(\hat{\mathbf{z}})$) constrained by the measurement error covariance matrix (\mathbf{S}_ϵ), and the second term
 28 accounting for the difference between retrieved ($\hat{\mathbf{z}}$) and a priori (\mathbf{z}_a) state vectors regulated
 29 by the a priori covariance matrix (\mathbf{S}_a).

1 Table 3 lists the sources for the a priori vector and covariance matrix for those parameters that
2 are being retrieved. The constraint matrix (S_a^{-1}) in equation 1 is to regularize the ill-posed
3 problem to obtain a stable solution that is an approximation to the exact solution. The
4 standard constraints for atmospheric retrievals include climatology and Tikhonov constraints.
5 The TES ozone retrievals use an altitude-dependent Tikhonov constraint matrix based on
6 minimizing the expected error over an ensemble of retrievals (Steck 2002; Kulawik et al.
7 2006c). [The altitude-dependent Tikhonov constraint, which is different from the classic](#)
8 [Tikhonov constraints, is composed of combinations of the zeroth-, first-, and second-order](#)
9 [Tikhonov constraints with altitude-dependent weights.](#) (Kulawik et al., 2006c). This
10 procedure was adopted because the TES retrieval algorithm development team empirically
11 found that low-thermal contrast conditions could result in many ozone retrievals showing
12 unphysical results, or retrievals with significantly large errors, near the surface.

13 For the joint TES and OMI retrieval we [used](#) a constraint matrix based on a climatology
14 generated using the MOZART3 (Brasseur et al., 1998; Park et al., 2004) ozone fields. The
15 climatological constraint, which has been used by Worden et al. (2007b) in the theoretical
16 study of combining TIR and UV ozone observations, provides a weaker constraint than the
17 altitude-dependent Tikhonov constraint matrix used in TES retrievals. This weaker constraint
18 is justified because the OMI radiances provide increased sensitivity to stratospheric ozone and
19 complimentary sensitivity (to TES) in the lower troposphere. In addition, we expect that the
20 sensitivity of the OMI radiances to the total tropospheric ozone column, along with little
21 sensitivity to thermal contrast [variations](#), will stabilize the ozone estimates near the surface
22 (see Section 4.1). For the OMI only retrievals, we [used](#) the same altitude-dependent Tikhonov
23 constraint matrix for ozone as that of TES retrievals. [We also tested the performances of TES](#)
24 [retrievals perform using the climatological based constraint.](#) Results for this comparison are
25 discussed in more detail in Section 4.1; we [found](#) that, as expected, the DOFS [improves](#) for
26 these TES ozone retrievals but the error also increases.

27 In addition to retrieving ozone concentration profiles (in volume mixing ratio or VMR), other
28 geophysical parameters that affect the observed radiances such as surface albedo and
29 emissivity, cloud properties, H₂O and temperature must also be estimated. Instrument
30 parameters such as OMI instrument wavelengths shifts must also be estimated for the UV
31 radiances. These parameters, and H₂O concentrations are all simultaneously estimated, along
32 with ozone for the joint TES/OMI retrieval. However, in addition to the initial guess for the

1 trace gas concentration, the initial guess for auxiliary parameters used in the simulation of
2 TIR radiances (including surface temperature, surface emissivity, cloud extinction, cloud top
3 pressure) were also obtained from TES version 4 products in order to speed up the
4 convergence of retrievals. Other parameters in the initial guess for the state vector were set
5 equal to the a priori constraint vector (surface albedo, wavelength shifting parameters, cloud
6 fraction).

7 Retrievals typically converged within 3-4 iterations and with Chi-square values (equation 1)
8 in the range of 1.2 to 1.3. A Chi square value of 1 indicates that the differences between
9 observed and simulated radiances are within measurement noise level, and the differences
10 between retrieved and a priori state vectors are within the a priori uncertainty.

11 **4 Results**

12 **4.1 Retrieval Characterization Example**

13 If the retrieval has converged and it can be shown that small changes in atmospheric state
14 result in small and linear changes in the modeled radiances, then the estimated state vector $\hat{\mathbf{z}}$
15 can be written as the linear expression (Rodgers 2000):

16

$$17 \quad \hat{\mathbf{z}} = \mathbf{z}_a + \mathbf{A}_{zz} [\mathbf{z}_{\text{true}} - \mathbf{z}_a] + \mathbf{G} \varepsilon + \delta_{cs}, \quad (2)$$

18

19 where \mathbf{z}_a is the a priori constraint vector, \mathbf{A}_{zz} is the averaging kernel matrix whose rows
20 represent the sensitivity of the retrieval to the true state, \mathbf{z}_{true} is the true state vector, ε is the
21 spectral noise, and \mathbf{G} is the gain matrix. The “cross-state” error, δ_{cs} , (Worden et al., 2007a) is
22 incurred from retrieving multiple parameters (e.g., water vapor, surface temperature, cloud
23 extinction and top pressure in TIR, cloud fraction in UV, surface albedo, and wavelength
24 shifting parameters). The trace of the averaging kernel matrix gives the number of
25 independent pieces of information in the vertical profile, or, the Degrees of Freedom for
26 Signal (DOFS) (Rodgers, 2000). A larger DOFS value indicates a better sensitivity.

27 Figure 1 shows sample averaging kernel matrices for TES, OMI and joint TES and OMI

1 observations over Naha, Okinawa, Japan on August 1st, 2007. These three measurements
 2 show different sensitivities to tropospheric ozone. TES can better resolve the lower/upper
 3 troposphere than OMI. Figure 1 shows the improvement in vertical resolution of tropospheric
 4 ozone by combining TES and OMI measurements. There is a clear enhancement of DOFS in
 5 the troposphere (TES only: 1.84; OMI only: 1.16; Joint TES and OMI: 2.21). The combined
 6 TES and OMI measurement also shows an increased sensitivity to the layer surface-700 hPa.
 7 In addition to the spring/summer season when the thermal contrast is usually high, these
 8 improvements have been also observed during the fall/winter season (Figure 2).

9 To validate the estimated ozone profiles, collocated ozonesonde measurements were
 10 compared to the estimated ozone profiles from TES only, OMI only, and joint TES and OMI
 11 measurements. The differences between the satellite retrievals and ozonesonde measurements
 12 smoothed by instrument averaging kernels can be written as (Worden et al., 2007a):

$$13 \quad \Delta_{\text{satellite-sonde}} = \hat{\mathbf{z}} - \hat{\mathbf{z}}_{\text{sonde}} = \mathbf{A}_{\text{zz}}[\mathbf{z} - \mathbf{z}_{\text{sonde}}] + \mathbf{G}\boldsymbol{\varepsilon} + \delta_{\text{cs}}, \quad (3)$$

14 where \mathbf{A}_{zz} represents the averaging kernels of TES, OMI, or combined TES and OMI
 15 measurements. \mathbf{z} , \mathbf{G} , $\boldsymbol{\varepsilon}$, and δ_{cs} are the state vector, gain matrix, the noise of measured
 16 radiances, and cross state error respectively. Equation 3 shows that the difference is not
 17 biased by the a priori constraint vector, \mathbf{z}_a , and can be used to identify other biases in ozone
 18 profiles estimated using satellite measurements (equation 4). The expected error for the
 19 differences between the satellite retrievals and ozonesonde measurements smoothed by
 20 instrument averaging kernels is:

$$21 \quad E\left[(\hat{\mathbf{z}} - \hat{\mathbf{z}}_{\text{sonde}})(\hat{\mathbf{z}} - \hat{\mathbf{z}}_{\text{sonde}})^T\right] = \underbrace{\mathbf{A}_{\text{zz}}\mathbf{S}_{\text{sonde}}\mathbf{A}_{\text{zz}}^T}_{\text{ozonesonde measurement Error}} + \underbrace{\mathbf{G}\mathbf{S}_{\boldsymbol{\varepsilon}}\mathbf{G}^T}_{\text{satellite instrument measurement error}} + \underbrace{\mathbf{A}_{\text{cs}}\mathbf{S}_{\text{cs}}\mathbf{A}_{\text{cs}}^T}_{\text{cross state error}}, \quad (4)$$

22 where \mathbf{A}_{cs} is the submatrix of the averaging kernel for the full state vector of all jointly
 23 retrieved parameters that relates the sensitivity of \mathbf{z} (the vector of cross-state parameters) to
 24 \mathbf{z}_{cs} (corresponding cross-state a priori constraint vector) (Worden et al., 2007a), $\mathbf{S}_{\text{sonde}}$ is the
 25 sonde error covariance, $\mathbf{S}_{\boldsymbol{\varepsilon}}$ is the spectral radiance measurement error covariance and \mathbf{S}_{cs} is
 26 the block diagonal matrix presented in equation 5. \mathbf{S}_{cs} contains the a priori covariance for the
 27 other jointly retrieved parameters including water vapor, surface temperature, surface

1 emissivity, cloud parameters in infrared (extinction and cloud top pressure), surface albedo in
 2 UV, wavelength shifting in UV, cloud parameter in UV (cloud fraction) parameters.

$$3 \quad \mathbf{S}_{cs} = \begin{pmatrix} \mathbf{S}_{\text{H}_2\text{O}} & \mathbf{0} \\ \mathbf{0} & \mathbf{S}_{\text{surf_TATM}} & \mathbf{0} & \mathbf{0} & \mathbf{0} & \mathbf{0} & \mathbf{0} & \mathbf{0} \\ \mathbf{0} & \mathbf{0} & \mathbf{S}_{\text{surf_emis}} & \mathbf{0} & \mathbf{0} & \mathbf{0} & \mathbf{0} & \mathbf{0} \\ \mathbf{0} & \mathbf{0} & \mathbf{0} & \mathbf{S}_{\text{cloud_IR}} & \mathbf{0} & \mathbf{0} & \mathbf{0} & \mathbf{0} \\ \mathbf{0} & \mathbf{0} & \mathbf{0} & \mathbf{0} & \mathbf{S}_{\text{surf_alb_UV}} & \mathbf{0} & \mathbf{0} & \mathbf{0} \\ \mathbf{0} & \mathbf{0} & \mathbf{0} & \mathbf{0} & \mathbf{0} & \mathbf{S}_{\text{ring_UV}} & \mathbf{0} & \mathbf{0} \\ \mathbf{0} & \mathbf{0} & \mathbf{0} & \mathbf{0} & \mathbf{0} & \mathbf{0} & \mathbf{S}_{\text{wls_UV}} & \mathbf{0} \\ \mathbf{0} & \mathbf{S}_{\text{cloud_UV}} \end{pmatrix}. \quad (5)$$

4 The differences between satellite measurements and in situ measurements (equation 3) arise
 5 from three sources: ozonesonde measurement error ($\sim\pm 5\%$, Worden et al., 2007a), satellite
 6 measurement error ($\sim\pm 15\text{-}20\%$ in the troposphere; $\sim\pm 5\text{-}10\%$ in the stratosphere), and cross-
 7 state error ($\sim\pm 15\text{-}20\%$ in the troposphere; $\sim\pm 5\text{-}10\%$ in the stratosphere). The sum of the last
 8 two terms is defined as observational error, which is the major contribution to the differences.
 9 Hence, for this analysis, we neglected the errors associated with the sonde measurements
 10 ($\pm 5\%$) since they are significantly smaller than the error terms of the satellite measurements.
 11 The typical altitude range of an ozonesonde measurement is from surface to above 10 hPa.
 12 [The unmeasured part of the stratosphere is approximated by appending the ozone a priori](#)
 13 [VMR](#). We neglected the [approximation in the stratosphere](#) that is applied in some sonde cases
 14 since the effects to the troposphere are minor. In addition, the above error estimation assumes
 15 that both the satellite instruments and sonde [measure](#) the same atmospheric state (or airmass).

16 Figures 3 and 4 show the ozone concentration profiles measured by sonde, TES and OMI
 17 instruments over Naha, Okinawa, Japan on August 1st, 2007 and Wallops Island, Virginia,
 18 USA on October 2nd, 2007, respectively. Both the sonde profiles smoothed by the averaging
 19 kernels of the satellite instruments (blue lines) and the estimated profiles (green lines) closely
 20 match the original ozonesonde measurements (black lines) and differ from the a priori
 21 profiles. Among the three sets of satellite measurements, the estimation using joint TES and
 22 OMI radiances has the smallest differences to the in situ measurements, [indicating enhanced](#)
 23 [sensitivities and reduced uncertainties in the measurements, especially in the altitude range](#)
 24 from the surface to about 300 hPa.

1 In the altitude range of 300 hPa to 100 hPa (Figures 3 and 4), the joint TES and OMI
2 retrievals show larger errors than the TES-only or OMI-only measurements. The current
3 discrepancy between UV and TIR spectroscopic parameters together with the radiometric
4 calibration consistency among different spectral regions are two major systematic error
5 sources that might affect the accuracy of joint TES and OMI retrievals. In addition, the
6 contribution of these two error sources can depend on pressure or temperature variations and
7 hence altitude. The spectral discrepancy between UV and TIR is generally about 5.5%
8 (Picquet-Varrault et al., 2005). The actual effect of the inconsistent UV and TIR
9 spectroscopic parameters and the radiometric calibrations is much less than the predicted
10 impacts shown in a previous study (Kulawik et al., 2007), possibly because fitting the surface
11 albedo parameters in the UV spectral region provides a zero order correction to the
12 radiometric calibration inconsistency (if there is any) between the TIR and UV spectral
13 regions. In addition, we applied the wavelength-dependent radiance calibration factors to the
14 OMI measurements prior to the joint TES and OMI retrievals. Those radiance calibration
15 factors were derived and validated by Liu et al. (2010a) for the OMI retrievals. The retrieved
16 profiles from joint retrievals do not show obvious ‘jackknifing’ features (Figures 3 and 4),
17 which usually appear when inconsistency of spectroscopic parameters and the radiometric
18 calibrations between TIR and UV spectral region severely affects the retrievals.

19 We next evaluated the bias and precision of each retrieval by showing comparisons between
20 TES, OMI, and the joint TES/OMI ozone profile estimates with all 22 sondes for the altitude
21 range between the surface and 700 hPa as well as from 700 to 100 hPa. As discussed
22 previously, the joint TES/OMI retrievals used a climatological constraint with relaxed
23 sensitivity near the surface and the OMI and TES retrievals used a Tikhonov-like constraint.
24 The corresponding averaging kernel and constraint vector were applied to the ozonesonde
25 profile prior to comparison in order to remove the effect of the retrieval regularization on the
26 comparison. Figure 5 shows that the bias and precision for the TES/OMI estimate is
27 $9.71\% \pm 26.06\%$. For TES and OMI alone the bias and precision are $9.04\% \pm 23.71\%$ and
28 $18.52\% \pm 36.99\%$ respectively.

29 The predicted precision for the TES/OMI estimates for the altitude range of 300 hPa to 100
30 hPa is 20.8% as compared to the actual precision of 26.06%; however, a lower calculated
31 precision was expected due to the non-linearity of the retrieval. For example, Boxe et al.
32 (2008) found that the vertical distribution of the calculated TES ozone precision is consistent

1 with the actual precision (as determined through comparison with ozonesondes) but is always
2 larger by an amount that varies between 1% to 10%. For the 700 hPa to 100 hPa region, all
3 instruments show similar **capability**. The actual precision for the TES/OMI estimates is
4 $6.5\% \pm 11.7\%$ and the calculated precision is 11.5%. We note that these precisions do not
5 describe how well each retrieval can resolve variations in tropospheric ozone because the
6 averaging kernel has been applied to the sondes prior to comparison. We **performed**
7 comparisons in the next section that test the capability of each retrieval for resolving
8 variations at each altitude.

9 The previous comparisons were not exactly an “apples-to-apples” comparison because a
10 climatological constraint was used for the joint TES/OMI retrievals whereas a Tikhonov-like
11 constraint **was** used for the TES and OMI retrievals. Theoretically, use of a climatological
12 constraint will increase the sensitivity of the TES and OMI retrievals to near-surface ozone
13 concentrations; however, as discussed earlier, the constraint used for the TES retrievals was
14 designed to reduce error in the lower troposphere resulting from degeneracy between thermal
15 contrast, surface emissivity, and near-surface ozone variations. We next **tested** whether this
16 climatological constraint could increase the information content of the TES retrievals. **We**
17 **found that the DOFS in the lower troposphere increases but the error in the retrieval increases**
18 **as well. For example, Figure 6 shows that the bias increases but the precision in the lower**
19 **troposphere decreases from $9\% \pm 23.7\%$ to $16.56\% \pm 39.7\%$.** This test **showed** that the joint
20 OMI/TES retrieval indeed increases both the sensitivity and information content of near-
21 surface ozone estimates over TES retrievals alone. We **did** not apply this test to the OMI
22 retrievals because the OMI ozone retrievals cannot resolve different parts of the troposphere.

23 **4.2 Comparisons of Ozone Observations among TES, OMI, Joint TES and** 24 **OMI, Ozone sonde**

25 Figure 7 shows the improvement in sensitivity to ozone for those TES-OMI pairs that
26 spatiotemporally **coincided** with the ozonesonde measurements (Table 2). **We calculated the**
27 **DOFS between the surface and 700 hPa (Figure 7, bottom panel) to estimate the sensitivity of**
28 **the ozone estimate to ozone near surface.** The sensitivity improvement by combining TES and
29 OMI radiances ranges from 30% to about a factor of 3, compared to each instrument alone.
30 When combining both TIR and UV radiances to estimate the ozone concentration, the
31 differences in the sensitivity characteristics between TES and OMI measurements enhance the

1 capability of distinguishing the middle tropospheric ozone from the lower tropospheric ozone.
2 TES averaging kernels present two peaks (Figures 1 and 2), one in the lower/middle
3 troposphere and the other in the lower stratosphere. In the troposphere, the peak altitudes of
4 TES averaging kernels slightly vary with pressure level while OMI averaging kernels almost
5 do not change. In addition, TES has stronger sensitivity in the middle and upper troposphere,
6 compared to that of OMI. The peaks of the averaging kernel present an altitude offset
7 between TES and OMI observations. TES is strongly peaked in the lower/middle troposphere,
8 whereas the OMI averaging kernels have peak sensitivity typically below the altitude where
9 the TES ozone estimate is most sensitive. This offset helps the combination of TES and OMI
10 better distinguish near surface ozone. The middle panel of Figure 7 shows the DOFS for the
11 region between the surface and 100 hPa and indicates that the improvement in vertical
12 resolution for this set of scenes ranges between 20% and 60%. The major part of the
13 improvement appears in the free troposphere below 300 hPa, where TES and OMI averaging
14 kernels show the greatest sensitivity to tropospheric ozone (Figures 1 and 2). Figure 7
15 presents the DOFS from three altitude ranges (top panel: surface to the top of atmosphere,
16 middle panel: troposphere, bottom panel: surface to 700 hPa) for three different measurement
17 approaches. TES shows better sensitivity in the troposphere than OMI since the DOFS of TES
18 measurements are larger than those of OMI (Figure 7 middle panel) in the troposphere,
19 whereas in the stratosphere the OMI observations show better sensitivity than TES as
20 indicated from the differences in DOFS between top and middle panels in Figure 7. When
21 combined TES and OMI radiances are used in the retrievals, DOFS are enhanced in both the
22 troposphere and the stratosphere, additionally there is improved separation between the
23 tropospheric and stratospheric ozone compared to using each instrument alone.

24 To further investigate the improvements on the tropospheric ozone sounding using both TIR
25 and UV bands, we ran retrievals using a common a priori ozone profile for all of the scenes in
26 Table 2 and compared the estimated ozone concentration to the ozonesonde measurements.
27 Using a fixed a priori profile helps interpret the variability of the retrieved ozone profiles. The
28 combined TES and OMI measurements (Figures 8–9) show a better correlation with the
29 ozonesondes than the TES or OMI measurements alone. Further, the root mean square of
30 fractional differences between retrievals and sonde measurements are significantly reduced
31 (by about a factor of 2) compared to either TES or OMI measurements alone, indicating that
32 the combined retrievals have better capability to capture the O₃ variation near the surface.

1 4.3 Further algorithm improvements

2 Joint TES and OMI retrievals exhibit enhanced sensitivity to ozone throughout the entire
3 altitude range. It is worth noting that sensitivity to [ozone near surface](#) has not been fully
4 exploited from the joint TES and OMI measurements due to the retrieval dependencies with
5 other ancillary parameters, especially for the wavelength-dependent surface albedo (OMI) and
6 emissivity (TES) parameters together with cloud fraction (OMI). Similar to the retrieval
7 algorithm developed by Liu et al. (2010a), in the OMI UV-2 spectral region (312–330 nm) we
8 fit a first-order wavelength dependent surface albedo term, which correlates (correlation
9 coefficient 0.2–0.5) with ozone concentration parameters, especially in the troposphere. On
10 the other hand, this parameter is needed in the retrieval to account partly for spectral
11 signatures of aerosol, clouds and calibration and helps to reduce fitting residuals. To reduce
12 the correlation between surface albedo and ozone concentration parameters and improve the
13 retrieval accuracy, we plan to implement a two-step approach in the retrieval algorithm: first,
14 we will retrieve surface albedo (a priori uncertainty: zero order term 0.05, first order term
15 0.01) and other ancillary parameters from the OMI ground pixels adjacent to those being used
16 in the joint TES and OMI observations; retrieved ancillary parameters from the first step will
17 then be used as initial guess along with an a priori constraint vector with reduced a priori
18 uncertainties (e.g, a priori uncertainty of surface albedo: zero order term 0.01, first order term
19 0.002) to estimate ozone concentration using combined TES and OMI measured radiances.
20 Reducing the a priori uncertainty decreases the correlation between ancillary parameters and
21 ozone concentration parameters. It also decreases the correlation among ancillary parameters
22 between surface albedo terms and cloud fraction, and between zero-order and first-order
23 radiance/ozone cross-section wavelength shifts in both UV-1 and UV-2.

24 [Our joint retrieval algorithm utilizes spatiotemporally coincident measured spectral radiances](#)
25 [to retrieve the vertical distribution of ozone concentration. The spectral radiances from 312 to](#)
26 [330 nm were coadded using measurements over two OMI UV-2 ground pixels prior to the](#)
27 [spectral fitting yielding a group pixel size of \$13 \times 48 \text{ km}^2\$ \(along ground track \$\times\$ cross ground](#)
28 [track of spacecraft\) at Nadir. The co-addition approach, which has been used by Liu et al.](#)
29 [\(2010a\) in OMI retrievals, helps in reducing forward model computation time compared to](#)
30 [simultaneously fitting UV-2 spectra that represent these ground pixels. It also ensures both](#)
31 [OMI UV1 and UV2 measurements probing common air volume, despite of introducing minor](#)
32 [spectral wavelength registration artifacts. A TES measurement at Nadir yields a ground pixel](#)

1 size of $8.5 \times 5.3 \text{ km}^2$ (along ground track \times cross ground track of spacecraft). We expect that
2 the differences on the size of ground pixels between TES and OMI measurements do not
3 significantly affect the retrieved ozone VMR since the measurements of using TIR spectral
4 region show most sensitivities over/above free troposphere where the spatial gradient of
5 ozone concentration are weak.

6 This work focused on investigating the feasibility of multiple spectral observations of near
7 surface ozone concentration, evaluating the performances using measured radiances from
8 current satellite instruments and providing realistic advance studies for the future missions.
9 Hence, the scenarios shown in this work are in the nearly clear sky conditions, in which the
10 cloud fraction in each instrument's field of view is less than 10%. We retrieved cloud
11 parameters for each instrument in order to account for the differences on the instrument's
12 field of view. Since both a priori values and initial guess values were taken from TES
13 standard products and OMI standard products, the jointly retrieved values are generally within
14 1% compared to the products from each instrument alone. When processing the entire TES
15 and OMI measured radiances that were recorded from 2005 to 2008, we decided to filter out
16 those scenes whose cloud fractions are greater than 30% using existing OMI released cloud
17 products. We expect that the future satellite missions can achieve improvements on
18 harmonizing the ground pixel sizes between TIR and UV bands, e.g., reducing the ground
19 pixel sizes of UV bands improves the number of cloud free scenes since both OMI and
20 GOME-2 provide larger ground pixels than TIR sounders onboard its common satellite
21 platform.

22 The estimated discrepancies of spectroscopic parameters between TIR and UV spectral
23 regions used in this work are up to 3%, which is smaller than the estimated measurement
24 uncertainties (Figure 5) and ozone natural variations near surface. To further improve the
25 quality of ozone measurements using multiple spectral regions, next generation of ozone
26 spectroscopic parameters should mitigate the existing **discrepancies** among different spectral
27 regions (microwave, thermal infrared, visible and ultraviolet). Prior to the availability of the
28 new ozone cross-sections that mitigate the existing discrepancy (3%) between UV and TIR
29 spectroscopic parameters, we will implement an alternative correction to the forward model
30 or retrieval, such as a retrieved or fixed line strength correction factor to address the
31 discrepancy on the spectroscopic parameters.

1

2 **5 Conclusions**

3 We have provided a demonstration of the first coincident multispectral retrievals of ozone
4 using both UV and TIR measured radiances from space. Improvements in both error
5 characteristics and vertical resolution compared to those without using multispectral retrievals
6 were shown. This technique allows for vertical ozone profiling with an average of 4.36 DOFS
7 in the stratosphere, 2.03 DOFS in the troposphere, and with sensitivity to the planetary
8 boundary layer (DOFS 0.37) for a wide variety of geophysical conditions. The typical
9 precision for a single target near-surface estimate of ozone is approximately 26% (15.6 ppb)
10 with a bias of approximately 9.6% (5.7 ppb). Comparison of the joint TES and OMI ozone
11 near-surface ozone estimates (surface to 700 hPa) to ozonesondes [shows enhanced capability](#)
12 in quantifying near-surface ozone variations over TES or OMI estimates alone. However,
13 improvements in vertical resolution are not as large as theoretically shown by Worden et al.
14 (2007) [due to](#) the need to retrieve ancillary parameters. To further improve the retrievals, we
15 need to reduce correlations between ozone concentration and ancillary parameters, improve
16 instrumental calibration, and perform more accurate radiative transfer calculations. [Additional](#)
17 [comparisons between OMI/TES profile estimates and ozone-sondes are desirable to gain](#)
18 [more confidence in these statistics.](#)

19

20 **Acknowledgements**

21 [We are grateful to Drs Ruud Dirksen, Robert Voors, and Marcel Dobbers for providing OMI](#)
22 [spectral slit function data and Dr Braak Remco at Royal Netherlands Meteorological Institute](#)
23 [for providing information on OMI L1b data.](#) We thank Drs. Annmarie Eldering, Stanley
24 Sander, Robert Herman, and Alyn Lambert for helpful discussions. We thank the World
25 Ozone Data Centre for making the routine sonde data accessible. [We thank the reviewers for](#)
26 [helpful suggestions.](#) The research described in this paper was carried out at the Jet Propulsion
27 Laboratory, California Institute of Technology, under a contract with the National
28 Aeronautics and Space Administration. Research at the Smithsonian Astrophysical
29 Observatory was supported by the National Aeronautics and Space Administration and by the
30 Smithsonian Institution. The JPL [authors'](#) copyright for this publication is held by the

1 California Institute of Technology. Government Sponsorship acknowledged.

2

3 **References**

4 Acarreta, J.R., De Haan, J.F., and Stammes P.: Cloud pressure retrieval using the O₂-O₂
5 absorption band at 477 nm, *J. Geophys. Res.*, 109, D05204, doi:10.1029/2003JD003915,
6 2004.

7 Akimoto, H., Irie, H., Kasai, Y., Kanaya, Y., Kita, K., Koike, M., Kondo, Y., Nakazawa, T.,
8 and Hayashida, S.: Planning a geostationary atmospheric observation satellite, Commission
9 on the Atmospheric Observation Satellite of the Japan Society of Atmospheric Chemistry,
10 2008. (<http://www.stelab.nagoya-u.ac.jp/ste-www1/div1/taikiken/eisei/eisei2.pdf>, Japanese
11 version only).

12 Bailey, P.L., Edwards, D.P., Gille, J.C., Lyjak, L.V., Massie, S.T., Roche, A.E., Kumer, J.B.,
13 Mergenthaler, J.L., Connor, B.J., Gunson, M.R., Margitan, J.J., McDermid, I.S., McGee, T.J.:
14 Comparison of cryogenic limb array etalon spectrometer (CLAES) ozone observations with
15 correlative measurements, *J. Geophys. Res.*, 101(D6), 9737–9756, doi:10.1029/95JD03614,
16 1996.

17 Beer, R.: Glavich, T.A., and Rider, D.M.: Tropospheric emission spectrometer for the Earth
18 Observing System's Aura satellite, *Appl. Opt.*, 40(15), 2356–2367,
19 doi:10.1364/AO.40.002356, 2001.

20 Beer, R., TES on the Aura mission: scientific objectives, measurements, and analysis
21 overview, *IEEE Transactions on Geoscience and remote sensing*, 44(5), 1102-1105, 2006.

22 Bell, M.L., Peng, R.D., and Dominici, F.: The Exposure–response curve for ozone and risk of
23 mortality and the adequacy of current ozone regulations, *Environ. Health Perspect.*, 114:532-
24 536, 2006.

25 Bernath, P.F., McElroy, C.T., Abrams, M.C., Boone, C.D., Butler, M., Camy-Peyret, C.,
26 Carleer, M., Clerbaux, C., Coheur, P.F., Colin, R., DeCola, P., DeMazière, M., Drummond,
27 J.R., Dufour, D., Evans, W.F.J., Fast, H., Fussen, D., Gilbert, K., Jennings, D.E., Llewellyn,
28 E.J., Lowe, R.P., Mahieu, E., McConnell, J.C., McHugh, M., McLeod, S.D., Michaud, R.,

1 Midwinter, C., Nassar, R., Nichitiu, F., Nowlan, C., Rinsland, C.P., Rochon, Y.J., Rowlands,
2 N., Semeniuk, K., Simon, P., Skelton, R., Sloan, J.J., Soucy, M.-A., Strong, K., Tremblay, P.,
3 Turnbull, D., Walker, K.A., Walkty, I., Wardle, D.A., Wehrle, V., Zander, R., and Zou, J.:
4 Atmospheric Chemistry Experiment (ACE): Mission overview, *Geophys. Res. Lett.*, 32,
5 L15S01, doi:10.1029/2005GL022386, 2005.

6 Bhartia, P.K., McPeters, R.D., Mateer, C.L., Flynn, L.E., and Wellemeyer, C.: Algorithm for
7 the estimation of vertical ozone profiles from the backscattered ultraviolet technique, *J.*
8 *Geophys. Res.*, 101(D13), 18793-18806, doi:10.1029/96JD01165, 1996.

9 Blom, C.E., Fischer, H., Glatthor, N., Gulde, T., Höpfner, M., and Piesch, C.: Spatial and
10 temporal variability of ClONO₂, HNO₃, and O₃ in the Arctic winter of 1992/1993 as obtained
11 by airborne infrared emission spectroscopy, *J. Geophys. Res.*, 100(D5), 9101-9114,
12 doi:10.1029/94JD02954, 1995.

13 Boone, C.D., Nassar, R., Walker, K.A., Rochon, Y., McLeod, S.D., Rinsland, C.P., and
14 Bernath, P.F.: Retrievals for the atmospheric chemistry experiment Fourier-transform
15 spectrometer, *Appl. Opt.*, 44(33), 7218-7231, doi:10.1364/AO.44.007218, 2005.

16 Bowman, K.W., Steck, T., Worden, H.M., Worden, J., Clough, S. and Rodgers, C.D.:
17 Capturing time and vertical variability of Tropospheric ozone: a study using TES nadir
18 retrieval, *J. Geophys. Res.*, 107(D23), doi:10.1029/2002JD002150, 2002.

19 Bowman, K.W., Rodgers, C.D., Kulawik, S.S., Worden, J., Sarkissian, E., Osterman, G.,
20 Steck, T., Lou, M., Eldering, A., Shephard, M., Worden, H., Lampel, M., Clough, S., Brown,
21 P., Rinsland, C., Gunson, M., Beer, R.: Tropospheric Emission Spectrometer: retrieval
22 method and error analysis, *IEEE Trans. Geosci. Remote Sensing*, 44, 1297-1307, 2006.

23 Boxe, C. S., Worden, J. R., Bowman, K. W., Kulawik, S. S., Neu, J. L., Ford, W. C.,
24 Osterman, G. B., Herman, R. L., Eldering, A., Tarasick, D. W., Thompson, A. M., et al.:
25 Validation of northern latitude Tropospheric Emission Spectrometer stare ozone profiles with
26 ARC-IONS sondes during ARCTAS: sensitivity, bias and error analysis, *Atmospheric*
27 *Chemistry and Physics*, 10(20), 9901–9914, doi:10.5194/acp-10-9901-2010, 2010.

1 Brasseur, G.P., Hauglustaine, D.A., Walters, S., Rasch, P.J., Muller, J.F., Granier, C., and Tie,
2 X.X.: MOZART, a global chemical transport model for ozone and related chemical tracers 1.
3 Model description, *J. Geophys. Res.*, 103(D21), doi:10.1029/98JD02397, 1998.

4 Brühl, C., Drayson, S.R., Russell, III J.M., Crutzen, P.J., McInerney, J.M., Purcell, P.N.,
5 Claude, H., Gernandt, H., McGee, T.J., McDermid, I.S., Gunson, M.R.: Halogen Occultation
6 Experiment ozone channel validation, *J. Geophys. Res.*, 101(D6), doi:10.1029/95JD02031,
7 1996.

8 Brion, J., Chakir, A., Daumont, D., and Malicet, J.: High-resolution laboratory absorption
9 cross section of O₃: Temperature effect, *Chem. Phys. Lett.*, 213(5-6), 610-612, doi:
10 10.1016/0009-2614(93)89169-I, 1993.

11 Browell, E.V., Carter, A.F., Shipley, S.T., Allen, R.J., Butler, C.F., Mayo, M.N., Siviter, J.
12 H., Jr., and Hall, W.M.: NASA Multipurpose Airborne DIAL system and measurements of
13 ozone and aerosol profiles, *Appl. Opt.*, 22(4), doi:10.1364/AO.22.000522, 1983.

14 Cai, Z., Liu, Y., Liu, X., Chance, K.V., Nowlan, C.R., Lang, R., Munro, R., Suleiman, R.:
15 Characterization and correction of Global Ozone Monitoring Experiment 2 ultraviolet
16 measurements and application to ozone profile retrievals, *J. Geophys. Res.*, 117, doi:
17 10.1029/2011JD017096, 2012.

18 Chance, K.V., Burrows, J.P., Perner, D., and Scheider, W.: Satellite measurements of
19 atmospheric ozone profiles, including tropospheric ozone, from ultraviolet/visible
20 measurements in the nadir geometry: a potential method, *J. Quant. Spectrosc. Radiat.*
21 *Transfer*, 57(4), doi:10.1016/S0022-4073(96)00157-4, 1997.

22 Clarmann, T.V., Oelhaf, H., and Fischer, H.: Retrieval of atmospheric O₃, HNO₃, CFC-11,
23 and CFC-12 profiles from MIPAS-B-89 limb emission spectra, *Appl. Opt.*, 32(33),
24 doi:10.1364/AO.32.006808, 1993.

25 Clerbaux, C., Turquety, S., Coheur, P.F.: Infrared remote sensing of atmospheric composition
26 and air quality: Towards operational applications, *Comptes Rendus Geosciences*, 342 (4-5),
27 349-356, doi:10.1016/j.crte.2009.09.010, 2010.

1 Clough, S.A., Shephard, M.W., Worden, J., Brown, P.D., Worden, H.M., Luo, M., Rodgers,
2 C.D., Rinsland, C.P., Goldman, A., Brown, L., Kulawik, S.S., Eldering, A., Lampel, M.C.,
3 Osterman, G., Beer, R., Bowman, K., Cady-Pereira, K.E., Mlawer, E.J.: Forward model and
4 Jacobians for Tropospheric Emission Spectrometer retrievals, *IEEE Trans. Geosci. Remote*
5 *Sensing*, 44, 1308-1323, 2006.

6 Cuesta, J., Eremenko, M., Liu, X., Dufour, G., Cai, Z., Höpfner, M., von Clarmann, T.,
7 Sellitto, P., Forêt, G., Gaubert, B., Beekmann, M., Orphal, J., Chance, K., Spurr, R., and
8 Flaud, J.-M.: Satellite observation of lowermost tropospheric ozone by multispectral
9 synergism of IASI thermal infrared and GOME-2 ultraviolet measurements, *Atmos. Chem.*
10 *Phys. Discuss.*, 13, 2955-2995, 2013.

11 Dobber, M.R., Dirksen, R.J., Levelt, P.F., van den Oord, G.H.J., Voors, R.H.M., Kleipool, Q.,
12 Jaross, G., Kowalewski, M., Hilsenrath, E., Leppelmeier, G.W., J. de Vries, Dierssen, W., and
13 Rozemeijer, N.C.: Ozone Monitoring Instrument calibration, *IEEE Trans. Geosci. Remote*
14 *Sens.*, 44, 1209-1238, 2006.

15 Eldering, A., Kulawik, S.S., Worden, J., Bowman, K., and Osterman, G.: Implementation of
16 cloud retrievals for TES atmospheric retrievals: 2. Characterization of cloud top pressure and
17 effective optical depth retrievals, *J. Geophys. Res.*, 113, D16S37,
18 doi:10.1029/2007JD008858., 2008.

19 Eichmann, K.-U., Kaiser J.W., von Savigny, C., Rozanov, A., Rozanov, V.V., Bovensmann,
20 H., von König, M., Burrows, J.P.: SCIAMACHY limb measurements in the UV/Vis spectral
21 region: first results, *Adv. Space Res.*, 34(4), 775-779, doi: 10.1016/j.asr.2003.05.057, 2004.

22 European Space Agency: GMES sentinels 4 and 5. Mission Requirements Document EOP-
23 SMA/1507, 87, 2007.

24 Fishman, J., Iraci, L.T., Al-Saadi, J., Chance, K., Chavez, F., Chin, M., Coble, P., Davis, C.,
25 DiGiacomo, P.M., Edwards, D., Eldering, A., Goes, J., Herman, J., Hu, C., Jacob, D., Jordan,
26 C., Kawa, S.R., Key, R., Liu, X., Lohrenz, S., Mannino, A., Natraj, V., Neil, D., Neu, J.,
27 Newchurch, M., Pickering, K., Salisbury, J., Sosik, H., Subramaniam, A., Tzortziou, M.,
28 Wang, J., Wang, M.: The United States' next generation of atmospheric composition and
29 coastal ecosystem measurements: NASA's Geostationary Coastal and Air Pollution Events

1 (GEO-CAPE) mission, Bull. Am. Meteorol. Soc., 93, 1547-1566, doi:10.1175/BAMS-D-11-
2 00201.1., 2012.

3 Flaud, J.-M., Piccolo, C., Carli, B., Perrin, A., Coudert, L.H., Teffo, J.-L., and Brown, L.R.:
4 Molecular line parameters for the MIPAS (Michelson Interferometer for Passive Atmospheric
5 Sounding) experiment (in Russian and English), Atmos. Oceanic Opt., 16, 172–182, 2003.

6 Götz, F.W.P., Meetham, A.R., and Dobson, G.M.B.: The vertical distribution of ozone in the
7 atmosphere, Proc. Roy. Soc. London, A145, 416-446, 1934.

8 Gunson, M.R., Farmer, C.B., Norton, R.H., Zander, R., Rinsland, C.P., Shaw, J.H., and Gao,
9 B.C.: Measurements of CH₄, N₂O, CO, H₂O, and O₃ in the middle atmosphere by the
10 Atmospheric Trace Molecule Spectroscopy experiment on Spacelab 3, J. Geophys. Res.,
11 95(D9), doi:10.1029/JD095iD09p13867, 1990.

12 Hamdouni, A., Barbe, A., Demoulin, P., and Zander, R.: Retrieval of ozone vertical column
13 amounts from ground-based high resolution infrared solar spectra, J. Quant. Spectrosc.
14 Radiat. Transfer, 57, 11-22, doi:10.1016/S0022-4073(96)00112-4, 1997.

15 Hatfield, J., Boote, K., Fay, P., Hahn, L., Izaurrealde, C., Kimball, B.A., Mader, Morgan, T.J.,
16 Ort D., Polley, W., Thomson, A., and Wolfe, D.: Agriculture. In: *The Effects of Climate*
17 *Change on Agriculture, Land Resources, Water Resources, and Biodiversity in the United*
18 *States* [Backlund, P., Janetos, A., Schimel, D., Hatfield, J., Boote, K., Fay, P., Hahn, L.,
19 Izaurrealde, C., Kimball, B.A., Mader, T., Morgan, J., Ort, D., Polley, W., Thomson, A.,
20 Wolfe, D., Ryan, M.G., Archer, S.R., Birdsey, R., Dahm, C., Heath, L., Hicke, J., Hollinger,
21 D., Huxman, T., Okin, G., Oren, R., Randerson, J., Schlesinger, W., Lettenmaier, D., Major,
22 D., Poff L., Running, S., Hansen, L., Inouye, D., Kelly, B.P., Meyerson, L., Peterson, B., and
23 Shaw, R. (eds.)]. Synthesis and Assessment Product 4.3. U.S. Department of Agriculture,
24 Washington, DC, pp. 21-74, 2008.

25 Hoogen, R., Rozanov, V.V., and Burrows, J.P.: Ozone profiles from GOME satellite data:
26 Algorithm description and first validation, J. Geophys. Res., 104(D7),
27 doi:10.1029/1998JD100093, 1999.

28 Ingmann, P., Veihelmann, B., Langen, J., Lamarre, D., Stark, H., Courrèges-Lacoste, G.B.:
29 Requirements for the GMES Atmosphere Service and ESA's implementation concept:

1 Sentinels-4/-5 and -5p, *Remote Sensing of Environment*, 120, 58-69, 2012, doi:
2 10.1016/j.rse.2012.01.023.

3 Jerrett, M., Burnett, R.T. and Pope, C.A. III, and Ito, K., Thurston, G. and Krewski, D. and
4 Shi, Y., Calle, E., and Thun, M.: Long-Term Ozone Exposure and Mortality, *N. Engl. J. Med.*
5 360 (11): 1085–1095, 2009.

6 Joiner, J. and Vasilkov, A.P.: First results from the OMI rotational raman scattering cloud
7 pressure algorithm, *IEEE T. Geosci. Remote*, 44, doi: 10.1109/TGRS.2005.861385, 2006.

8 Kalnay, E., Kanamitsu, M., Kistler, R., Collins, W., Deaven, D., Gandin, L., Iredell, M., Saha,
9 S., White, G., Woollen, J., Zhu, Y., Chelliah, M., Ebisuzaki, W., Higgins, W., Janowiak, J.,
10 Mo, K.C., Ropelewski, C., Wang, J., Leetmaa, A., Reynolds, R., Jenne, R., and Joseph, D.:
11 The NCEP/NCAR 40-year reanalysis project, *B. Am. Meteorol. Soc.*, 77(3), 437–471, 1996.

12 Kleipool, Q.L., Dobber, M.R., Haan, J. F. de, and Levelt, P. F.: Earth surface reflectance
13 climatology from 3 years of OMI data, *J. Geophys. Res.*, 113, doi: 10.1029/2008JD010290,
14 2008.

15 Komhyr, W.D., Barnes, R.A., Brothers, G.B., Lathrop, J.A., and Opperman, D.P.:
16 Electrochemical concentration cell ozonesonde performance evaluation during STOIC 1989,
17 *J. Geophys. Res.*, 100(D5), doi:10.1029/94JD02175, 1995.

18 Kroon, M., de Haan, J.F., Veefkind, J.P., Froidevaux, L., Wang, R., Kivi, R., and
19 Hakkarainen, J.J.: Validation of operational ozone profiles from the Ozone Monitoring
20 Instrument, *J. Geophys. Res.*, 116, D18305, doi:10.1029/2010JD015100, 2011.

21 Kuai, L., Worden, J., Kulawik, S., Bowman, K., Biraud, S., Abshire, J. B., Wofsy, S. C.,
22 Natraj, V., Frankenberg, C., Wunch, D., Connor, B., Miller, C., Roehl, C., Shia, R.-L., and
23 Yung, Y.: Profiling tropospheric CO₂ using the Aura TES and TCCON instruments, *Atmos.*
24 *Meas. Tech. Discuss.*, 5, 4495-4534, doi:10.5194/amtd-5-4495-2012, 2012.

25 Kulawik, S.S., Worden, H., Osterman, G., Luo, M., Beer, R., Kinnison, D.E., Bowman, K.W.,
26 Worden, J., Eldering, A., Lampel, M., Steck, T., Rodgers, C.D.: TES Atmospheric Profile
27 Retrieval Characterization: An Orbit of Simulated Observations, *IEEE Trans. Geosci. Remote*
28 *Sensing*, 44, 1324-1333, May 2006a.

- 1 Kulawik, S.S., Worden, J., Eldering, A., Bowman, K., Gunson, M., Osterman, G.B., Zhang,
2 L., Clough, S., Shephard, M.W., Beer, R.: Implementation of cloud retrievals for
3 Tropospheric Emission Spectrometer (TES) atmospheric retrievals: part 1. Description and
4 characterization of errors on trace gas retrievals, *J. Geophys. Res.*, 111, D24204,
5 doi:10.1029/2005JD006733, 2006b.
- 6 Kulawik, S.S., Osterman, G., and Jones, D.: Calculation of altitude-dependent Tikhonov
7 constraints for TES nadir retrievals, *IEEE Trans. Geosci. Remote Sens.*, 44(5), 1334–1342,
8 May 2006c.
- 9 Kulawik, S.S., Liu, X., Worden, J.R., Chance, K., Bowman, K., Worden, H., and the TES
10 team: Optimally combining ozone from Tropospheric Emission Spectrometer (TES) and
11 Ozone Monitoring Instrument (OMI) data. *Eos, Transactions, American Geophysical Union*
12 88(52), Fall Meeting Supplement, Abstract A33C-1403, 2007.
- 13 Lahoz, W.A., Peuch, V.-H., Orphal, J., Attié, J.-L., Chance, K., Liu, X., Edwards, D., Elbern,
14 H., Flaud, J.-M., Claeysman, M., and El Amraoui, L.: Monitoring air quality from space: The
15 case for the geostationary platform, *Bull. Amer. Meteorol. Soc.*, doi: 10.1175/BAMS-D-11-
16 00045.1, 221-233, 2012.
- 17 Landgraf, J. and Hasekamp, O.P.: Retrieval of tropospheric ozone: The synergistic use of
18 thermal infrared emission and ultraviolet reflectivity measurements from space, *J. Geophys.*
19 *Res.*, 112, D08310, doi:10.1029/2006JD008097, 2007.
- 20 Lee, S., Hong, Y., Song, C.-K., Lee, J., Choi, W.-J., Kim, D., Moon, K.-J., and Kim, J.: Plan
21 of Korean Geostationary Environment Satellite over Asia-Pacific region: Geophysical
22 Research Abstracts, Vol. 12, EGU2010-7595-1, EGU General Assembly, 2010.
- 23 Liu, X., Chance, K., Sioris, C.E., Spurr, R.J.D., Kurosu, T.P., Martin, R.V., and Newchurch
24 M.J.: Ozone profile and tropospheric ozone retrievals from the Global Ozone Monitoring
25 Experiment: Algorithm description and validation, *J. Geophys. Res.*, 110, D20307,
26 doi:10.1029/2005JD006240, 2005.
- 27 Liu, X., Chance, K., Sioris, C.E., Kurosu, T.P., Spurr, R.J.D., Martin, R.V., Fu, T.M, Logan,
28 J.A., Jacob, D.J., Palmer, P.I., Newchurch, M.J., Megretskaja, I.A., and Chatfield, R.B.: First
29 directly retrieved global distribution of tropospheric column ozone from GOME: Comparison

1 to the GEOS-Chem model, *J. Geophys. Res.*, 111, D02308, doi:10.1029/2005JD006564,
2 2006.

3 Liu, X., Chance, K., Sioris, C.E., and Kurosu, T.P.: Impact of using different ozone cross
4 sections on ozone profile retrievals from Global Ozone Monitoring Experiment (GOME)
5 ultraviolet measurements, *Atmos. Chem. Phys.*, 7, 3571-3578, doi:10.5194/acp-7-3571-2007,
6 2007.

7 Liu, X., Bhartia, P.K., Chance, K., Spurr, R.J.D., and Kurosu, T.P.: Ozone profile retrievals
8 from the Ozone Monitoring Instrument, *Atmos. Chem. Phys.*, 10, 2521–2537,
9 doi:10.5194/acp-10-2521-2010, 2010a.

10 Liu, X., Bhartia, P.K., Chance, K., Froidevaux, L., Spurr, R.J.D., and Kurosu, T.P.:
11 Validation of Ozone Monitoring Instrument (OMI) ozone profiles and stratospheric ozone
12 columns with Microwave Limb Sounder (MLS) measurements, *Atmos. Chem. Phys.*, 10,
13 2539-2549, doi:10.5194/acp-10-2539-2010, 2010b.

14 Livesey, N. J., Filipiak, M. J., Froidevaux, L., Read, W. G., Lambert, A., Santee, M. L., Jiang,
15 J. H., Pumphrey, H. C., Waters, J. W., Cofield, R. E., Cuddy, D. T., Daffer, W. H., Drouin, B.
16 J., Fuller, R. A., Jarnot, R. F., Jiang, Y. B., Knosp, B. W., Li, Q. B., Perun, V. S., Schwartz,
17 M. J., Snyder, W. V., Stek, P. C., Thurstans, R. P., Wagner, P. A., Avery, M., Browell, E. V.,
18 Cammas, J. P., Christensen, L. E., Diskin, G. S., Gao, R. S., Jost, H. J., Loewenstein, M.,
19 Lopez, J. D., N'ed'elec, P., Osterman, G. B., Sachse, G. W., and Webster, C. R.: Validation
20 of Aura Microwave Limb Sounder O₃ and CO observations in the upper troposphere and
21 lower stratosphere, *J. Geophys. Res.*, 113, D15S02, doi:10.1029/2007JD008805, 2008.

22 McConnell, J., McElroy, C.T., Solheim, B., Sioris, C., Evans, W., Buijs, H., Roux, M.,
23 Rahnema, P., Walker, K., Jones, D., Garand, L., Nassar, R., Martin, R., O'Neill, N.,
24 Bergeron, M., and the PCW/PHEMOS Science Team: A quasi-geostationary view of the
25 Arctic and environs: PCW/PHEMOS for Arctic weather, climate and air quality,
26 EUMETSAT meteorological satellite conference, Oslo, Norway, 2011.

27 McDermid, I.S., Beyerle, G., Haner, D.A., and Leblanc, T.: Redesign and improved
28 performance of the tropospheric ozone lidar at the Jet Propulsion Laboratory Table Mountain
29 Facility, *Appl. Opt.*, 41(36), doi:10.1364/AO.41.007550, 2002.

1 McPeters, R.D., Janz, S.J., Hilsenrath, E., Brown, T.L., Flittner, D.E., and Heath, D.F.: The
2 retrieval of O₃ profiles from limb scatter measurements: Results from the Shuttle Ozone Limb
3 Sounding Experiment, *Geophys. Res. Lett.*, 27(17), 2597-2600, doi:10.1029/1999GL011342,
4 2000.

5 McPeters, R. D., Labow, G. J., and Logan, J. A.: Ozone climatological profiles for satellite
6 retrieval algorithms, *J. Geophys. Res.*, 112, D05308, doi:10.1029/2005JD006823, 2007.

7 Molod, A., Takacs L., Suarez, M., Bacmeister, J., Song, I., and Eichmann, A.: The GEOS-5
8 Atmospheric General Circulation Model: Mean Climate and Development from MERRA to
9 Fortuna, Tech. Rep. 28, Goddard Space Flight Center, NASA/TM-2012-104606, 2012.

10 Munro, R., Siddans, R., Reburn, W.J., and Kerridge, B.: Direct measurement of tropospheric
11 ozone from space, *Nature*, 392, 168-171, doi:10.1038/32392, 1998.

12 National Research Council, Committee on Earth Science and Applications from Space: A
13 Community Assessment and Strategy for the Future: Earth Science and Applications from
14 Space: National Imperatives for the Next Decade and beyond, National Academies Press,
15 Washington D.C., 2007.

16 Natraj, V., Liu, X., Kulawik, S., Chance, K., Chatfield, R., Edwards, D., Eldering, A.,
17 Francis, G., Kurosu, T., Pickering, K., Spurr, R., Worden, H.: Multi-spectral sensitivity
18 studies for the retrieval of tropospheric and lowermost tropospheric ozone from simulated
19 clear-sky GEO-CAPE measurements, *Atmospheric Environment*, 45(39),
20 doi:10.1016/j.atmosenv.2011.09.014, 2011.

21 Park, M., Randel, W.J., Kinnison, D.E., Garcia, R.R., and Choi, W.: Seasonal variation of
22 methane, water vapor, and nitrogen oxides near the tropopause: Satellite observations and
23 model simulations, *J. Geophys. Res., Atmos.*, 109, D03302, doi: 10.1029/2003JD003706.
24 2004.

25 Petropavlovskikh, I., Bhartia, P.K., and DeLuisi, J.: New Umkehr ozone profile retrieval
26 algorithm optimized for climatological studies, *Geophys. Res. Lett.*, 32, L16808,
27 doi:10.1029/2005GL023323, 2005.

1 Picquet-Varrault, B., Orphal, J., Doussin, J.-F., Carlier, P., Flaud, J.-M.: Laboratory
2 intercomparison of the ozone absorption coefficients in the mid-infrared (10 μm) and
3 ultraviolet (300 - 350 nm) spectral regions. *J. Phys. Chem. A.*, 109(6), 1008-1014,
4 doi:10.1021/jp0405411, 2005.

5 Pougatchev, N.S., Connor, B.J., and Rinsland, C.P.: Infrared measurements of the ozone
6 vertical distribution above Kitt Peak, *J. Geophys. Res.*, 100(D8), doi:10.1029/95JD01296,
7 1995.

8 Riese, M., Spang, R., Preusse, P., Ern, M., Jarisch, M., Offermann, D., and Grossmann, K.-
9 U.: Cryogenic Infrared Spectrometers and Telescopes for the Atmosphere (CRISTA) data
10 processing and atmospheric temperature and trace gas retrieval, *J. Geophys. Res.*, 104(D16),
11 doi:10.1029/1999JD900274, 1999.

12 Rodgers, C.D.: *Inverse methods for atmospheric sounding: Theory and practice*, World
13 Scientific Publishing, Singapore, 2000.

14 Rothman, L.S., Jacquemart, D., Barbe, A., Benner, D.C., Birk, M., Brown, L.R., Carleer,
15 M.R., Chackerian, C.Jr., Chance, K., Coudert, L.H., Dana, V., Devi, V.M., Flaud, J.-M.,
16 Gamache, R.R., Goldman, A., Hartmann, J.-M., Jucks, K.W., Maki, A.G., Mandin, J.-Y.,
17 Massie, S.T., Orphal, J., Perrin, A., Rinsland, C.P., Smith, M.A.H., Tennyson, J., Tolchenov,
18 R.N., Toth, R.A., Vander Auwera, J., Varanasi, P., Wagner, G.: The HITRAN 2004
19 molecular spectroscopic database, *J. Quant. Spectrosc. Radiat. Transfer*, 96(2), 139-204, doi:
20 10.1016/j.jqsrt.2004.10.008, 2005.

21 Rothman, L.S., Gordon, I.E., Barbe, A., Benner, C., Bernath, P.F., Birk, M., Boudon, V.,
22 Brown, L.R., Campargue, A., Champion, J.P., Chance, K., Coudert, L.H., Dana, V., Devi,
23 V.M., Fally, S., Flaud, J.M., Gamache, R.R., Goldman, A., Jacquemart, D., Kleiner, I.,
24 Lacombe, N., Lafferty, W. J., Mandin, J.Y., Massie, S.T., Mikhailenko, S.N., Miller, C.E.,
25 Moazzen-Ahmadi, N., Naumenko, O.V., Nikitin, A.V., Orphal, J., Perevalov, V.I., Perrin, A.,
26 Predoi Cross, A., Rinsland, C.P., Rotger, M., Simecková, M., Smith, M.A.H., Sung, K.,
27 Tashkun, S.A., Tennyson, J., Toth, R.A., Vandaele, A.C., and Auwera, J.V.: The HITRAN
28 2008 molecular spectroscopic database, *J. Quant. Spectrosc. Radiat. Transfer*, 110(9-10), 533-
29 572, doi: 10.1016/j.jqsrt.2009.02.013, 2009.

- 1 Sellitto, P., Frate, F.D., Solimini, D., Casadio, S.: Tropospheric Ozone Column Retrieval
2 From ESA-Envisat SCIAMACHY Nadir UV/VIS Radiance Measurements by Means of a
3 Neural Network Algorithm, *IEEE Transactions on Geosciences and Remote Sensing*, 50(3),
4 998-1011, 2012a.
- 5 Sellitto, P., Noia, A.D., Frate, F.D., Burini, A., Casadio, S., Solimini, D.: On the role of
6 visible radiation in ozone profile retrieval from nadir UV/VIS satellite measurements: An
7 experiment with neural network algorithms inverting SCIAMACHY data, *Journal of*
8 *Quantitative Spectroscopy and Radiative Transfer*, 113(12), 1429-1436, 2012b.
- 9 Sioris, C.E. and Evans, W.F.J.: Impact of rotational Raman scattering in the O₂ A band,
10 *Geophys. Res. Lett.*, 27(24), 4085-4088, doi:10.1029/2000GL012231, 2000.
- 11 Spurr, R.J.D.: VLIDORT: A linearized pseudo-spherical vector discrete ordinate radiative
12 transfer code for forward model and retrieval studies in multilayer multiple scattering media,
13 *J. Quant. Spectrosc. Radiat. Transfer*, 102, 316-342, doi:10.1016/j.jqsrt.2006.05.005, 2006.
- 14 Spurr, R.J.D.: Linearized pseudo-spherical scalar and vector discrete ordinate radiative trans-
15 fer models for use in remote sensing retrieval problems, in: *Light Scattering Reviews*, edited
16 by: Kokhanovsky, A., Springer, New York, Part II, 229–275, doi:10.1007/978-3-540-48546-
17 97, 2008.
- 18 Steck, T.: Methods for determining regularization for atmospheric retrieval problems, *Appl.*
19 *Opt.*, 41(9), 1788-1797, doi:10.1364/AO.41.001788, 2002.
- 20 Toon, G.C., Farmer, C.B., Lowes, L.L., Schaper, P.W., Blavier, J.-F., and Norton, R.H.:
21 Infrared Aircraft Measurements of Stratospheric Composition over Antarctica during
22 September 1987, *J. Geophys. Res.*, 94(D14), doi:10.1029/JD094iD14p16571, 1989.
- 23 Toon, G.C., Sen, B., Blavier, J.F., Sasano, Y., Yokota, T., Kanzawa, H., Ogawa, T., Suzuki,
24 M., and Shibasaki, K.: Comparison of ILAS and MkIV profiles of atmospheric trace gases
25 measured above Alaska in May 1997, *J. Geophys. Res.*, 107(D24), 8211,
26 doi:10.1029/2001JD000640, 2002.
- 27 Tzortziou, M., Krotkov, N., Cede, A., Herman, J., Vasilkov, A.: New technique for retrieval
28 of tropospheric and stratospheric ozone profiles using sky radiance measurements at multiple

1 view angles: application to a brewer spectrometer, *J. Geophys. Res.*, 113, D06304,
2 doi:10.1029/2007JD009093, 2008.

3 van Peet, J.C.A., van der A, R.J., de Laat, A.T.J., Tuinder, O.N.E., König-Langlo, G., and
4 Wittig, J.: Height resolved ozone hole structure as observed by the Global Ozone Monitoring
5 Experiment–2, *Geophys. Res. Lett.*, 36, L11816, doi:10.1029/2009GL038603, 2009.

6 von Savigny, C., Haley, C.S., Sioris, C.E., McDade, I.C., Llewellyn, E.J., Degenstein, D.,
7 Evans, W.F.J., Gattinger, R.L., Griffioen, E., Kyrölä, E., Lloyd, N.D., McConnell, J.C.,
8 McLinden, C.A., Mégie, G., Murtagh, D.P., Solheim, B., Strong, K.: Stratospheric ozone
9 profiles retrieved from limb scattered sunlight radiance spectra measured by the OSIRIS
10 instrument on the Odin satellite, *Geophys. Res. Lett.*, 30(14), 1755,
11 doi:10.1029/2002GL016401, 2003.

12 Vasilkov, A., Joiner, J., Spurr, R., Bhartia, P.K., Levelt, P., and Stephens, G.: Evaluation of
13 the OMI cloud pressures derived from rotational Raman scattering by comparisons with other
14 satellite data and radiative transfer simulations, *J. Geophys. Res.*, 113, D15S19, doi:
15 10.1029/2007JD008689, 2008.

16 Wagner, G., Birk, M., Schreier, F., and Flaud, J.-M.: Spectroscopic database for ozone in the
17 fundamental spectral regions, *J. Geophys. Res.*, 107, 4626, doi:10.1029/2001JD000818, 2002.

18 Weidner, F., Bösch, H., Bovensmann, H., Burrows, J.P., Butz, A., Camy-Peyret, C., Dorf, M.,
19 Gerilowski, K., Gurlit, W., Platt, U., von Friedeburg, C., Wagner, T., and Pfeilsticker, K.:
20 Balloon-borne limb profiling of UV/vis skylight radiances, O₃, NO₂, and BrO: technical set-
21 up and validation of the method, *Atmos. Chem. Phys.*, 5, 1409-1422, doi:10.5194/acp-5-
22 1409-2005, 2005.

23 Weinhold, B.: Ozone nation: EPA standard panned by the people, *Environ. Health Perspect.*
24 116 (7): A302–A305. 2008.

25 Worden, H.M, Beer, R., Bowman, K.W., Fisher, B., Luo, M., Rider, D., Sarkissian, E.,
26 Tremblay, D., Zong, J.: TES Level 1 Algorithms: Interferogram Processing, Geolocation,
27 Radiometric, and Spectral Calibration, *IEEE Trans. Geosci. Remote Sensing*, 44, 1288-1296,
28 2006.

1 Worden, H.M., Logan, J.A., Worden, J.R., Beer, R., Bowman, K., Clough, S.A., Eldering, A.,
2 Fisher, B.M., Gunson, M.R., Herman, R.L., Kulawik, S.S., Lampel, M.C., Luo, M.,
3 Megretskaia, I.A., Osterman, G.B., and Shephard M.W.: Comparisons of Tropospheric
4 Emission Spectrometer (TES) ozone profiles to ozonesondes: Methods and initial results, J.
5 Geophys. Res., 112, D03309, doi:10.1029/2006JD007258, 2007a.

6 Worden, J., Liu, X., Bowman, K., Chance, K., Beer, R., Eldering, A., Gunson, M., and
7 Worden, H.: Improved tropospheric ozone profile retrievals using OMI and TES radiances,
8 Geophys. Res. Lett., 34, L01809, doi:10.1029/2006GL027806, 2007b.

9 Worden, H.M., Deeter, M.N., Edwards, D.P., Gille, J.C., Drummond, J.R., and Nédélec,
10 P.: Observations of near-surface carbon monoxide from space using MOPITT multispectral
11 retrievals, J. Geophys. Res., 115, D18314, doi:10.1029/2010JD014242, 2010.

12 World Health Organization: Health Aspects of Air Pollution with Particulate Matter, Ozone
13 and Nitrogen Dioxide, Bonn, Germany, 13–15 January 2003.

14

15

16

17

18

19

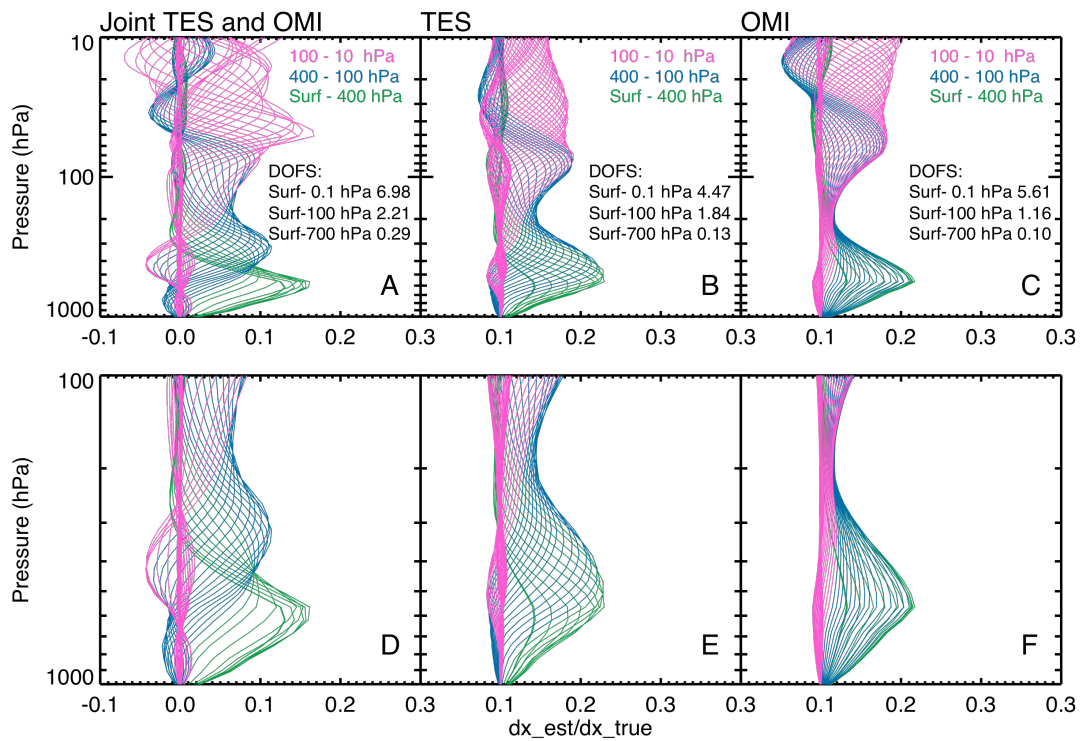
20

21

22

23

24

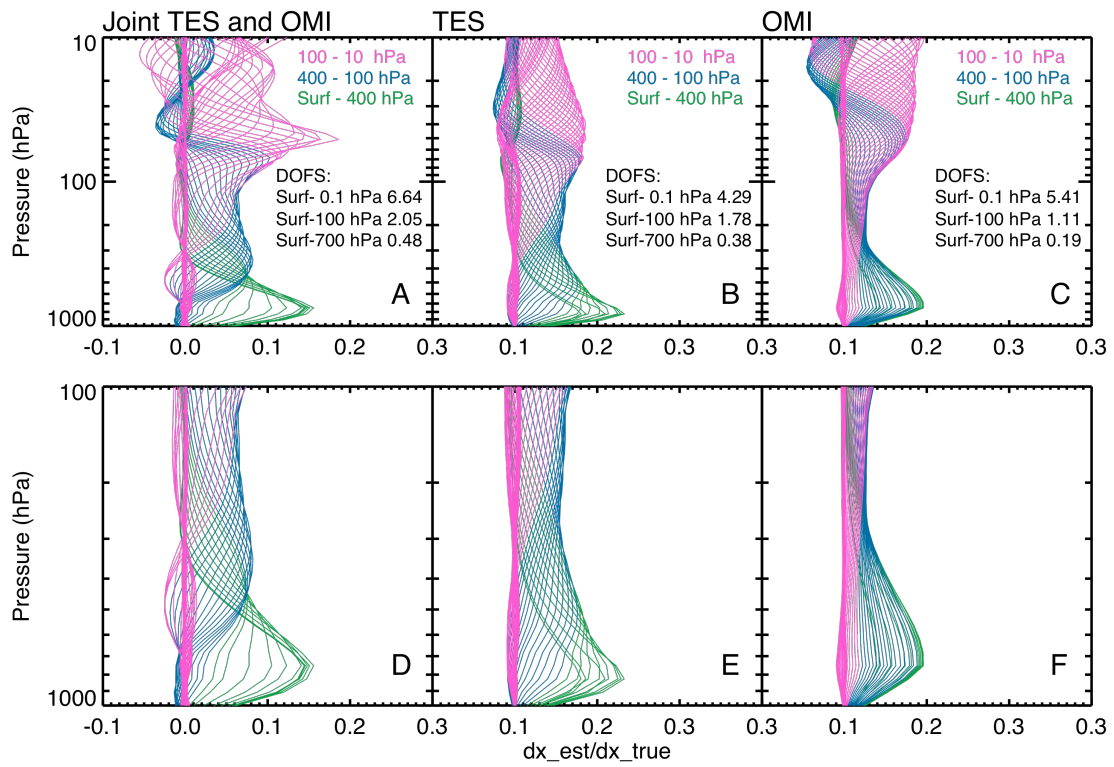


1

2 **Figure 1.** Examples of averaging kernels for the measurement over Naha, Okinawa, Japan on
 3 August 1st, 2007: (A) Joint TES and OMI measurement; (B) TES measurement; (C) OMI
 4 measurement; (D, E, F) zoom-in view of averaging kernels from surface to 100 hPa.

5

6



1

2 **Figure 2.** Examples of averaging kernels for the measurement over Wallops Island, Virginia,
 3 USA on October 2nd, 2007: (A) Joint TES and OMI measurement; (B) TES measurement; (C)
 4 OMI measurement; (D, E, F) zoom-in averaging kernels from surface to 100 hPa.

5

6

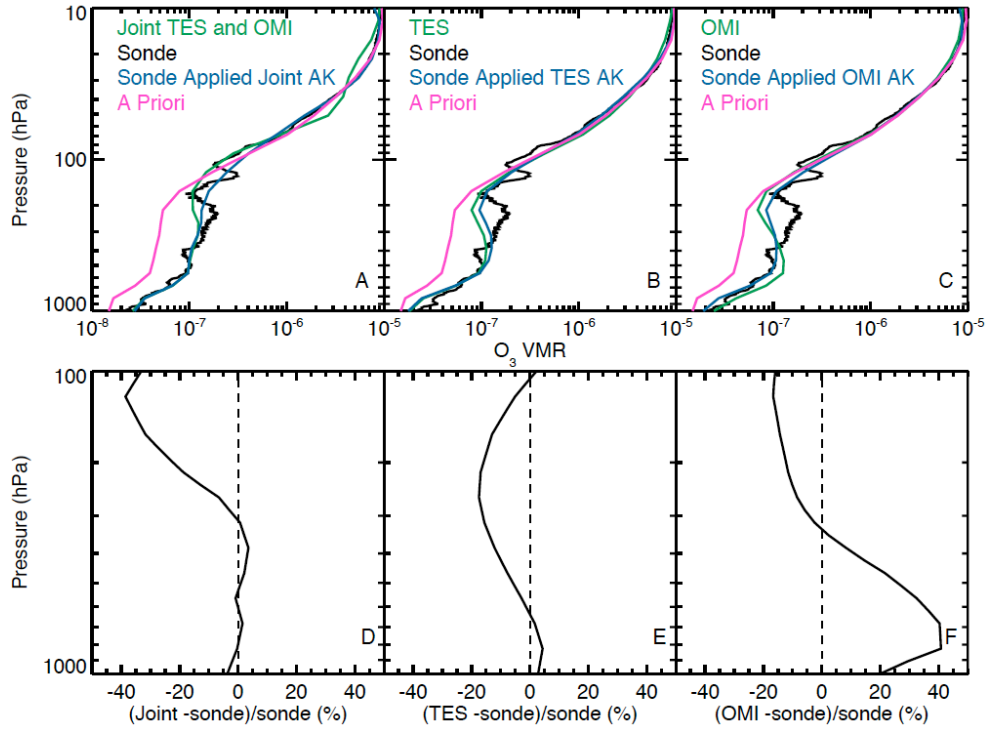
7

8

9

10

11



1

2 **Figure 3.** Ozone volume mixing ratios measured by the instruments on Aura satellite and
 3 ozonesonde over Naha, Okinawa, Japan on August 1st, 2007. It is the same scenario as the one
 4 shown in Figure 1. (A) Joint TES and OMI vs. Ozonesonde; (B) TES only vs. Ozonesonde;
 5 (C) OMI only vs. Ozonesonde; (D) Percentage differences between joint retrieval and co-located
 6 sonde measurements; (E) Percentage differences between TES retrieval and co-located
 7 sonde measurements (F) Percentage differences between OMI retrieval and co-located
 8 sonde measurements. In Panels A, B and C, retrieved profiles in green; ozonesonde
 9 sonde measurements are in black; ozonesonde profiles smoothed by averaging kernels of TES or
 10 OMI in blue; A priori in magenta.

11

12

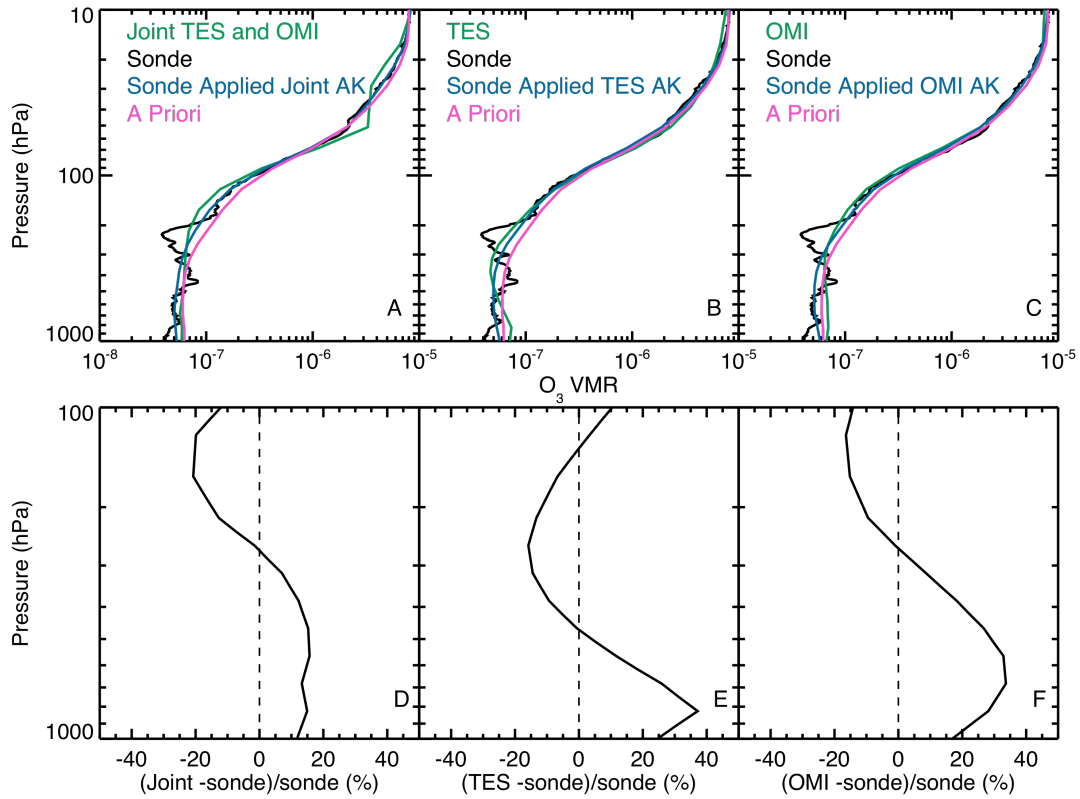
13

14

15

16

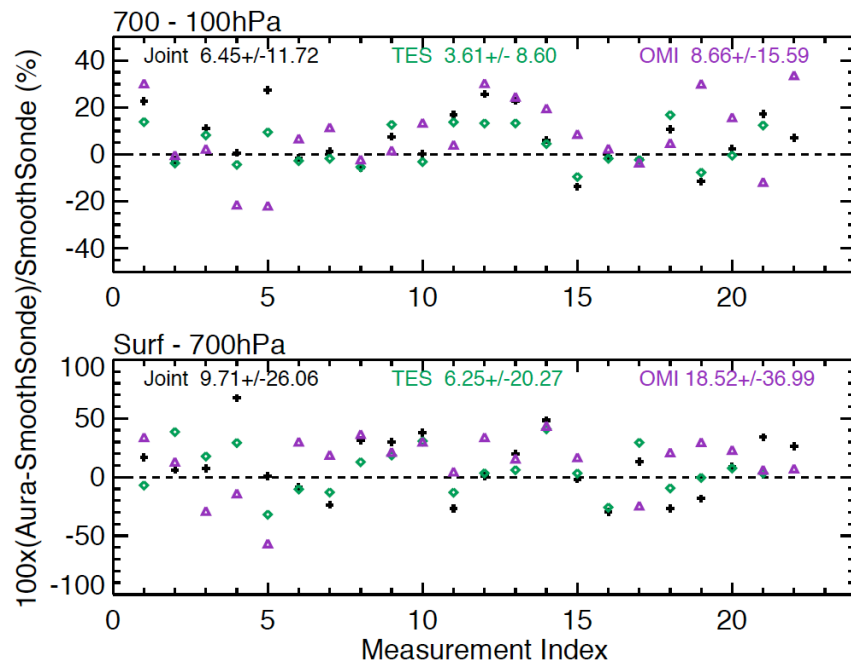
1
2
3



4

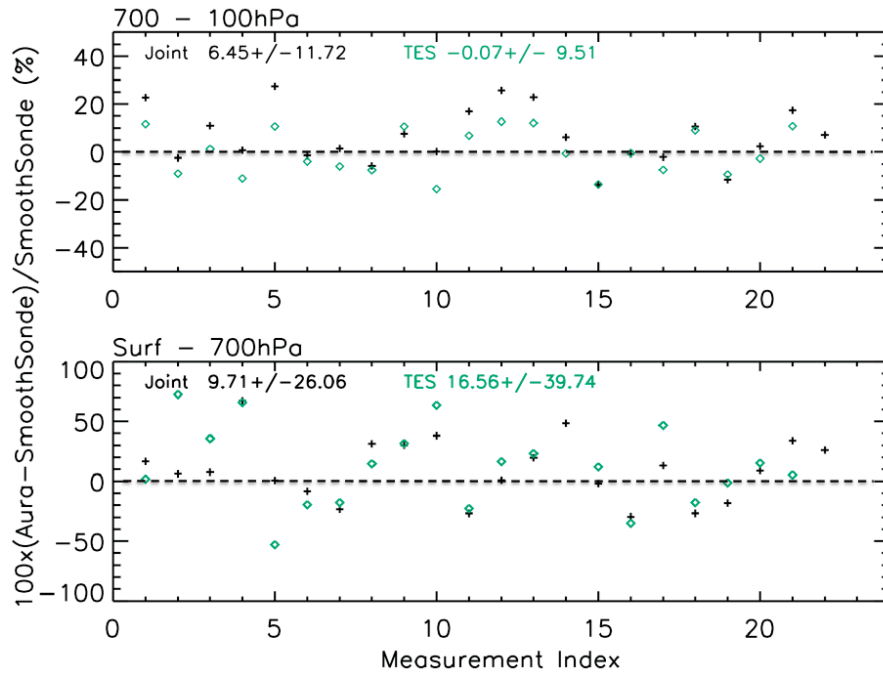
5 **Figure 4.** Ozone volume mixing ratios measured by the instruments on Aura satellite and
6 ozonesonde over Wallops Island, Virginia, USA on October 2nd, 2007. It is the same scenario
7 as the one shown in Figure 2. (A) Joint TES and OMI vs. Ozonesonde; (B) TES only vs.
8 Ozonesonde; (C) OMI only vs. Ozonesonde; (D) Percentage differences between joint
9 retrieval and co-located sonde measurements; (E) Percentage differences between TES
10 retrieval and co-located sonde measurements (F) Percentage differences between OMI
11 retrieval and co-located sonde measurements. In Panels A, B and C, retrieved profiles
12 in green; ozonesonde measurements are in black; ozonesonde profiles smoothed by averaging
13 kernels of TES or OMI in blue; A priori in magenta.

14



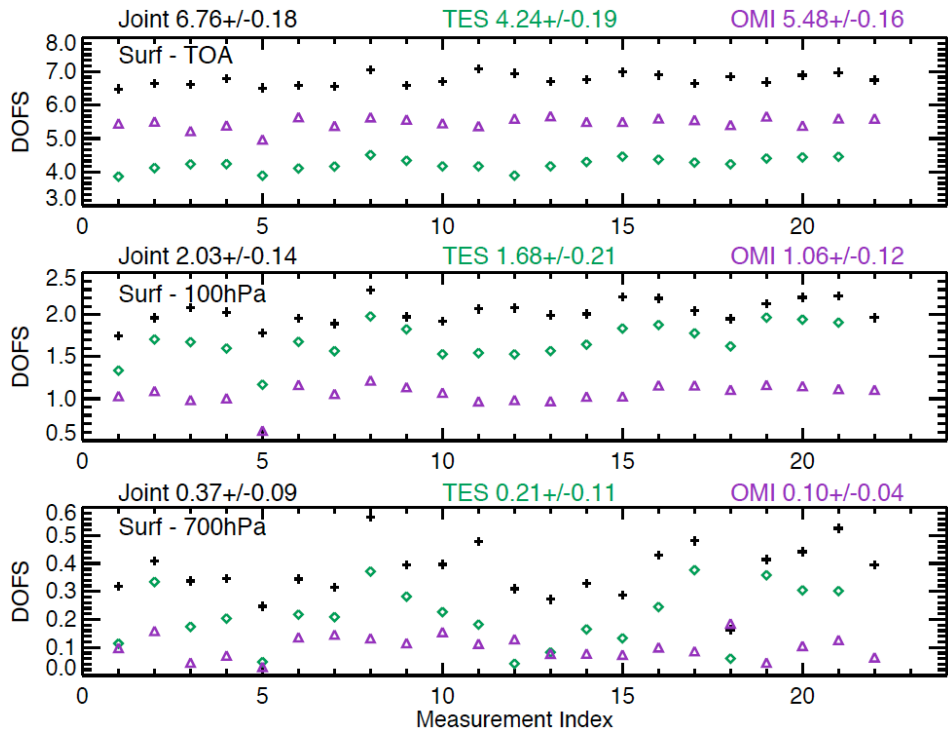
1
2
3
4
5
6
7
8
9

Figure 5. Percentage differences between coincident Aura measurements and ozonesonde measurements in the troposphere: joint TES and OMI (black plus), TES only (green diamond), OMI only (purple triangle). The joint TES and OMI retrievals used the constraint matrix created from the MOZART3 ozone climatological covariance. The TES only and OMI only used an altitude-dependent Tikhonov constraint matrix. A priori ozone profile varies for each scene. The measurement index in the X axis is given in Table 2. The averaging kernels of Aura measurements were applied to the ozonesonde measurements.



1
2
3
4
5
6
7
8
9

Figure 6. Percentage differences between Aura measurements and ozonesonde measurements in the troposphere: Joint TES and OMI (black plus), TES only (green diamonds). The TES only together with joint TES and OMI retrievals use the constraint matrix created from the MOZART3 ozone climatological covariance. The measurement index in the X axis is given in Table 2. A priori ozone profile varies for each scene. The averaging kernels of Aura measurements are applied to the ozonesonde measurements.



1

2 **Figure 7.** DOFS for the set of ozone measurements in Table 2: (Top panel) total DOFS;
 3 (Middle panel) DOFS for the region between the surface and 100 hPa; (Bottom panel) DOFS
 4 for the region between surface to 700 hPa; Joint OMI and TES (black plus); TES (green
 5 diamond); OMI (purple triangle).

6

7

8

9

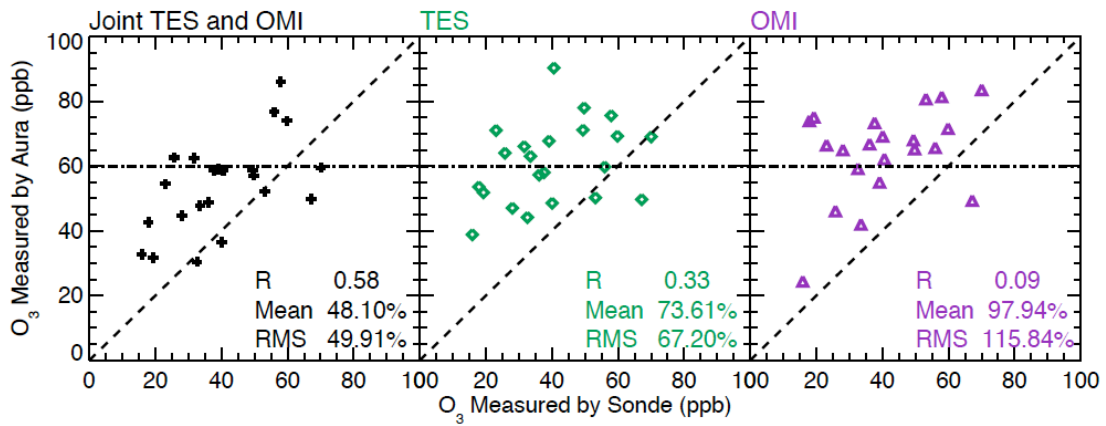
10

11

12

13

14



1

2 **Figure 8.** Correlations of Aura measured and ozonesonde measured ozone concentration
 3 (parts-per-billion) in the region from surface to 700 hPa: joint TES and OMI (left panel); TES
 4 only (middle panel); OMI only (right panel). The joint observations have improved the
 5 capability of capturing the variations of ozone concentration in the region from surface to 700
 6 hPa, compared to TES or OMI observations alone. A common a priori ozone profile
 7 (horizontal dash line) was used in the retrievals for all of the scenes. The black dotted dash
 8 line indicates one to one correlation. The averaging kernels of the Aura measurements were
 9 not applied to the ozonesonde measurements.

10

11

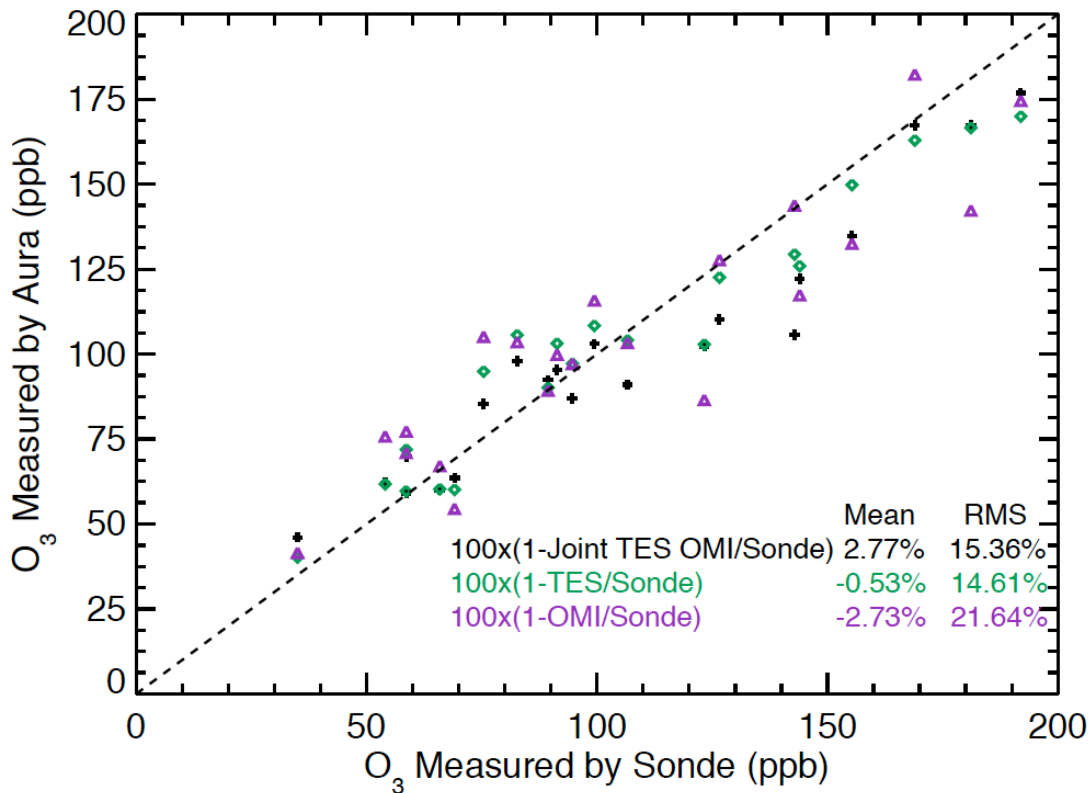
12

13

14

15

16



1

2 **Figure 9.** Correlations of Aura measured and ozonesonde measured ozone concentration
 3 (parts-per-billion) in the region from 700 hPa to 100 hPa: Joint OMI and TES (black plus);
 4 TES (green diamond); OMI (purple triangle). The discrepancy between joint observations and
 5 sonde measurements is larger (Mean: 1.24%; RMS: 0.75%) than that between TES only
 6 measurements and sonde measurements. Both Joint observations and TES only measurements
 7 show better agreement to sonde measurements than OMI only measurements. A common a
 8 priori ozone profile was used in the retrievals for all of the scenes. The averaging kernels of
 9 Aura measurements were not applied to the ozonesonde measurements.

1 **Table 1.** Spectral Regions used in Joint TES and OMI Ozone Retrievals.

Data Source	Optical Filter	Start Frequency	End Frequency	Point Spacing ¹	Atmospheric Species
TES	IB2	990.02 cm ⁻¹	1031.12 cm ⁻¹	0.06 cm ⁻¹	O ₃ , H ₂ O, CO ₂
TES	IB2	1044.08 cm ⁻¹	1049.06 cm ⁻¹	0.06 cm ⁻¹	O ₃ , H ₂ O, CO ₂
TES	IB2	1068.98 cm ⁻¹	1071.38 cm ⁻¹	0.06 cm ⁻¹	O ₃ , H ₂ O, CO ₂
TES	2A1	1172.56 cm ⁻¹	1176.22 cm ⁻¹	0.06 cm ⁻¹	O ₃ , H ₂ O, HDO, CO ₂ , CH ₄ , N ₂ O
TES	2A1	1184.62 cm ⁻¹	1189.36 cm ⁻¹	0.06 cm ⁻¹	O ₃ , H ₂ O, HDO, CO ₂ , CH ₄ , N ₂ O
TES	2A1	1195.12 cm ⁻¹	1201.30 cm ⁻¹	0.06 cm ⁻¹	O ₃ , H ₂ O, HDO, CO ₂ , CH ₄ , N ₂ O
TES	2A1	1209.52 cm ⁻¹	1214.26 cm ⁻¹	0.06 cm ⁻¹	O ₃ , H ₂ O, HDO, CO ₂ , CH ₄ , N ₂ O
TES	2A1	1224.10 cm ⁻¹	1227.88 cm ⁻¹	0.06 cm ⁻¹	O ₃ , H ₂ O, HDO, CO ₂ , CH ₄ , N ₂ O
TES	2A1	1259.38 cm ⁻¹	1261.42 cm ⁻¹	0.06 cm ⁻¹	O ₃ , H ₂ O, HDO, CO ₂ , CH ₄ , N ₂ O
TES	2A1	1265.92 cm ⁻¹	1267.06 cm ⁻¹	0.06 cm ⁻¹	O ₃ , H ₂ O, HDO, CO ₂ , CH ₄ , N ₂ O
TES	2A1	1269.46 cm ⁻¹	1270.54 cm ⁻¹	0.06 cm ⁻¹	O ₃ , H ₂ O, HDO, CO ₂ , CH ₄ , N ₂ O
TES	2A1	1277.86 cm ⁻¹	1279.24 cm ⁻¹	0.06 cm ⁻¹	O ₃ , H ₂ O, HDO, CO ₂ , CH ₄ , N ₂ O
TES	2A1	1311.70 cm ⁻¹	1315.36 cm ⁻¹	0.06 cm ⁻¹	O ₃ , H ₂ O, HDO, CO ₂ , CH ₄ , N ₂ O
TES	2A1	1315.72 cm ⁻¹	1317.82 cm ⁻¹	0.06 cm ⁻¹	O ₃ , H ₂ O, HDO, CO ₂ , CH ₄ , N ₂ O
OMI	UV-1	270 nm	308 nm	0.32 nm	O ₃
OMI	UV-2	312 nm	330 nm	0.15 nm	O ₃

2 1. TES has a uniform spectral grid. The spectral point spacing of OMI is not constant and the mean value in the spectral region is listed.

3

4

1 **Table 2.** Coincident measurements among TES, OMI, and Ozoneonde.

Profile Index	Date	TES Ground Pixel Latitude	TES Ground Pixel Longitude	Cloud Optical Depth	Delta Time ¹ Minute	Distance Km	Measurement ² TES	Ozoneonde Site
1	2005-07-18	19.86°N	154.82°W	0.10	-12.6	24.29	Global Survey	Hilo
2	2005-08-25	37.94°N	76.21°W	0.05	40.1	19.81	Global Survey	Wallops Island
3	2006-01-10	19.89°N	154.81°W	0.03	-12.1	23.31	Global Survey	Hilo
4	2006-01-12	21.32°S	55.09°E	0.03	-3.7	36.35	Global Survey	Reunion Island
5	2006-01-25	0.85°S	90.09°W	0.02	-24.9	19.92	Transect	San Cristobal
6	2006-04-06	37.88°N	76.27°W	0.03	38.9	27.45	Global Survey	Wallops Island
7	2006-05-04	21.29°S	54.85°E	0.03	-3.8	35.61	Global Survey	Reunion Island
8	2006-08-28	37.91°N	76.30°W	0.06	40.2	28.28	Global Survey	Wallops Island
9	2006-09-29	37.94°N	76.29°W	0.01	22.4	26.24	Global Survey	Wallops Island
10	2006-10-25	19.85°N	154.98°W	0.03	-18.7	16.38	Global Survey	Hilo
11	2006-12-18	37.90°N	76.09°W	0.03	39.0	14.18	Global Survey	Wallops Island
12	2007-01-03	37.91°N	76.08°W	0.03	-3.0	12.16	Global Survey	Wallops Island
13	2007-05-21	19.88°N	154.95°W	0.03	-18.3	14.13	Global Survey	Hilo
14	2007-06-06	19.89°N	154.92°W	0.02	-18.6	14.41	Global Survey	Hilo
15	2007-08-01	26.28°N	127.79°E	0.00	-33.5	37.61	Global Survey	Naha
16	2007-08-31	37.91°N	76.28°W	0.06	34.0	26.44	Global Survey	Wallops Island
17	2007-10-02	37.94°N	76.30°W	0.04	27.2	26.94	Global Survey	Wallops Island
18	2008-07-09	26.34°N	128.19°E	0.02	-34.4	42.49	Global Survey	Naha
19	2008-07-23	38.35°N	76.00°W	0.02	42.5	38.77	Step & Stare	Wallops Island
20	2008-08-08	37.95°N	75.92°W	0.03	39.7	8.99	Step & Stare	Wallops Island
21	2008-08-16	35.13°N	87.47°W	0.01	15.9	45.18	Step & Stare	Huntsville
22	2008-10-29	25.63°N	128.24°E	0.02	-32.7	47.92	Global Survey	Naha

2 1. TES measurement time – Ozoneonde measurement time; **Time difference between collocated TES and OMI measurements is within seconds.**

3 2. **All OMI** measurements used here were taken from global measurement mode.

1 **Table 3.** List of fitting variables, *a priori* values and *a priori* errors.

Case Selection ¹	Fitting Parameters	Number of Parameters	<i>A Priori</i>	<i>A Priori</i> Uncertainty
TES+OMI, TES, OMI	O ₃ at each level	25	MOZART-3	MOZART-3
TES+OMI, TES	H ₂ O at each level	16	GEOS4	NCEP ~30%
TES+OMI, TES	Surface temperature ²	1	GEOS4	0.5K
TES+OMI, TES	Surface emissivity ²	32	ASTER and land use map	~0.006
TES+OMI, TES	Cloud extinction	10	Initial BT difference	300%
TES+OMI, TES	Cloud top pressure	1	500 mbar	100%
TES+OMI, OMI	UV-1 Surface Albedo	1	OMI climatology	0.05
TES+OMI, OMI	UV-2 Surface Albedo (zero order term)	1	OMI climatology	0.05
TES+OMI, OMI	First-order wavelength-dependent term for UV-2	1	0.0	0.01
TES+OMI, OMI	Ring scaling parameters	2	1.9	1.00
TES+OMI, OMI	Radiance/irradiance wavelength shifts	2	0.0	0.02 nm
TES+OMI, OMI	Radiance/O ₃ cross section wavelength shifts (zero order)	2	0.0	0.02 nm
TES+OMI, OMI	Radiance/O ₃ cross section wavelength shifts (first order)	2	0.0	0.004
TES+OMI, OMI	Cloud Fraction	1	Derived from 347 nm	0.05

2 1. The parameters are included in the retrievals for different cases (TES only, OMI only, and TES and OMI)

3 2. Retrievals over land, spectral surface emissivity and surface temperature are included.

4